
Doctoral Dissertations

Student Theses and Dissertations

Fall 2018

Modeling and experimental investigations on particle dynamic behaviors in laser 3D printing with blown powder

Wei Li

Follow this and additional works at: https://scholarsmine.mst.edu/doctoral_dissertations



Part of the [Mechanical Engineering Commons](#)

Department: Mechanical and Aerospace Engineering

Recommended Citation

Li, Wei, "Modeling and experimental investigations on particle dynamic behaviors in laser 3D printing with blown powder" (2018). *Doctoral Dissertations*. 2724.

https://scholarsmine.mst.edu/doctoral_dissertations/2724

This thesis is brought to you by Scholars' Mine, a service of the Missouri S&T Library and Learning Resources. This work is protected by U. S. Copyright Law. Unauthorized use including reproduction for redistribution requires the permission of the copyright holder. For more information, please contact scholarsmine@mst.edu.

MODELING AND EXPERIMENTAL INVESTIGATIONS ON PARTICLE DYNAMIC
BEHAVIORS IN LASER 3D PRINTING WITH BLOWN POWDER

by

WEI LI

A DISSERTATION

Presented to the Faculty of the Graduate School of the
MISSOURI UNIVERSITY OF SCIENCE AND TECHNOLOGY

In Partial Fulfillment of the Requirements for the Degree

DOCTOR OF PHILOSOPHY

in

MECHANICAL ENGINEERING

2018

Approved by:

Dr. Frank Liou, Advisor

Dr. Ashok Midha

Dr. Heng Pan

Dr. Lianyi Chen

Dr. Xiaoming He

© 2018

Wei Li

All Rights Reserved

PUBLICATION DISSERTATION OPTION

This dissertation consists of the following four articles that have been published or submitted for publication as follows:

Paper I. Pages 6-30 have been published in Journal of Materials Processing Technology.

Paper II. Pages 31-55 are intended for submission to Journal of Manufacturing Processes.

Paper III. Pages 56-71 have been published in International Journal of Advanced Manufacturing Technology.

Paper IV. Pages 72-88 are intended for submission to International Journal of Advanced Manufacturing Technology.

All of them have been prepared in the format of Missouri S&T specs.

ABSTRACT

Pre-mixed powder is frequently-used powder supply to fabricate Functional Gradient Material (FGM) by Laser 3D printing, which is also called Laser Metal Deposition (LMD). The deposited FGM composition is expected to be similar or same as supplied powder mixture. However, because pre-mixed powder has different particle densities and particle sizes, the caused particle acceleration differences can result in the separation in powder mixture. Up to now, there was no study focused on pre-mixed powders' flow behavior in LMD. The current research aims to investigate the flow behaviors of pre-mixed powder supplied for LMD through both experimental and modeling approaches. In this dissertation, four research achievements are introduced in detail as follows. First of all, an effective experimental method is utilized to investigate the powder fluid behaviors in powder mixture during flow in powder feeder pipe. Secondly, a comprehensive CFD-DEM model is built to simulate the powder mixture fluid behaviors and particle trajectory. This model can provide an effective method to analyze the powder separation phenomenon, the processing parameters' effects on the separation, etc. Thirdly, the effect of argon gas flow rate on the powder separation is studied through the CFD-DEM model and validated by the experiment results. Finally, based on the particle acceleration theory, a novel particle size optimization idea is introduced in the research. This optimization idea can control the powder separation and keep almost uniform powder mixture composition. The main contribution of this research is to solve the composition ratio deviation of pre-mixed powder in fabricating FGM through LMD process, in order to enhance the quality of FGM.

ACKNOWLEDGMENTS

First and foremost, I would like to express my sincere gratitude to my advisor, Dr. Frank Liou, for his encouragement, insightful guidance, and support during my PhD study at Missouri University of Science and Technology. He patiently guided me through every stage of my research while granted me a great deal of independence. His encouragement endowed me with tremendous confidence in exploring unknown scientific territory and challenging myself to be my best. His diligence and rigorous altitude to research and work will have a significant influence on my future life. It has been a privilege and a great honor to have worked with him.

I would also like to extend my appreciation to all my dissertation committee members, Dr. Ashok Midha, Dr. Heng Pan, Dr. Lianyi Chen and Dr. Xiaoming He. Without their guidance and valuable comments, it is impossible for me to complete my dissertation.

The dissertation was supported by the Laser Aided Manufacturing Processes (LAMP) Laboratory, and the Intelligent System Center of Missouri S&T, which are gratefully acknowledged.

I would like to express my deep thanks to my lab-mates and friends, Mr. Sreekar Karnati, Mr. Yunlu Zhang, Ms. Xueyang Chen, Mr. Jingwei Zhang, Mr. Xinchang Zhang and Mr. Lei Yan for their support during my study in Rolla.

Last but not the least, I wish to extend my special and sincere thanks to my parents and all the family members, for their love and unwavering supports.

TABLE OF CONTENTS

	Page
PUBLICATION DISSERTATION OPTION.....	iii
ABSTRACT.....	iv
ACKNOWLEDGMENTS	v
LIST OF ILLUSTRATIONS.....	ix
LIST OF TABLES.....	xi
 SECTION	
1. INTRODUCTION	1
1.1. BACKGROUND.....	1
1.2. RESEARCH OBJECTIVES.....	3
1.3. ORGANIZATION OF DISSERTATION.....	5
 PAPER	
I. INVESTIGATION AND ELIMINATING POWDER SEPARATION IN PRE- MIXED POWDER SUPPLY FOR LASER METAL DEPOSITION	6
ABSTRACT.....	6
1. INTRODUCTION.....	7
2. PARTICLE ACCELERATION ANALYSIS IN ARGON GAS FLOW.....	13
3. EXPERIMENT PROCEDURE.....	15
4. RESULTS AND DISCUSSION	21
4.1. ANALYSIS STEPS FOR THE EXPERIMENT RESULTS	22
4.2. RESULTS OF EXPERIMENT	23

5. CONCLUSION	28
REFERENCES	29
II. NUMERICALLY SIMULATING THE SEPARATION OF PRE-MIXED POWDER FLOW SUPPLIED FOR LASER METAL DEPOSITION AND EXPERIMENTAL VALIDATION	31
ABSTRACT.....	31
1. INTRODUCTION	32
2. CFD-DEM MODELING METHODOLOGY.....	35
3. MODELING PREPARATION	41
4. SIMULATION RESULTS AND DISCUSSION.....	44
5. EXPERIMENTAL VALIDATION	49
6. CONCLUSION	52
REFERENCES	53
III. MODELING ANALYSIS OF ARGON GAS FLOW RATE'S EFFECT ON PRE-MIXED POWDER SEPARATION IN LASER METAL DEPOSITION AND EXPERIMENTAL VALIDATION	56
ABSTRACT.....	56
1. INTRODUCTION.....	57
2. MODELING PROCEDURE.....	60
2.1. CALCULATION DOMAIN.....	60
2.2. POWDER DESCRIPTION AND OPERATING PARAMETERS.....	61
3. SIMULATION RESULTS AND DISCUSSION.....	62
4. EXPERIMENTAL VALIDATION	66
5. CONCLUSION	68
REFERENCES	69

IV. CFD-DEM MODELING ANALYSIS OF PARTICLE SIZE OPTIMIZATION'S EFFECT ON CONTROLLING PRE-MIXED POWDER FLOW SEPARATION IN LASER METAL DEPOSITION	72
ABSTRACT.....	72
1. INTRODUCTION.....	73
2. EXPERIMENTAL REVIEW AND PARTICLE SIZE OPTIMIZATION APPROACH INTRODUCTION	75
3. SIMULATION RESULTS AND DISCUSSION.....	81
4. CONCLUSION	86
REFERENCES	86
SECTION	
2. CONCLUSION.....	89
BIBLIOGRAPHY	91
VITA.....	93

LIST OF ILLUSTRATIONS

SECTION	Page
Figure 1.1. Customized material manufactured by Laser metal deposition	2
 PAPER I	
Figure 1. Schematic illustration of fabricating customized material by LMD	9
Figure 2. (a). VHN of four samples in sequence; (b). fresh mixed powders; (c). remaining mixed powders after prior two depositions; (d). remaining mixed powders after all the four depositions.	10
Figure 3. Two primary driving forces for particle.	14
Figure 4. Optical microscopic images for: (a) Cu particles; and (b) 4047 Al particles	17
Figure 5. Experiment set-up: (a) Schematic diagram; and (b) Work site	18
Figure 6. Two Pre-mixed powder patterns: (a) experiment-1; and (b) experiment-2.....	22
Figure 7. Observation of the experiment results.....	23
Figure 8. Six pre-mixed powder pattern zones in experiment-1	24
Figure 9. Pre-mixed powder volume percentage history in experiment-1.....	26
Figure 10. Six pre-mixed powder pattern zones in experiment-2.....	27
Figure 11. Pre-mixed powder volume percentage history in experiment-2.....	27
 PAPER II	
Figure 1. Two primary driving forces for particle	37
Figure 2. Modeling set-up: (a) calculation domain; (b) real situation in lab	42
Figure 3. Optical microscopic images for: (a) Cu particles; and (b) 4047 Al particles	43
Figure 4. The powder distribution in simulation result.....	45

Figure 5. Ten sections in feeder pipe	46
Figure 6. The simulated powder distribution in the ten pipe sections	46
Figure 7. The powder distribution in section1 at different moments.....	48
Figure 8. The powder distribution in section3 at different moments.....	48
Figure 9. Powder quantification results	48
Figure 10. Experiment set-up and powder volume percent quantification.....	50
Figure 11. Experimentally validating the simulation result.....	52
PAPER III	
Figure 1. Schematic illustration of fabricating customized material by LMD	59
Figure 2. Ten sections in feeder pipe	63
Figure 3. Simulated powder distribution in the ten pipe sections at the moment of 5s. ...	64
Figure 4. Powder quantification results	65
Figure 5. Experimental validating the model.....	67
PAPER IV	
Figure 1. Schematic illustration of feeding process of pre-mixed powders.	75
Figure 2. Optical microscopic images for: (a) Cu particles; and (b) 4047 Al particles....	77
Figure 3. (a). Experiment design; (b). Experiment set-up; (c). Powder volume percent quantification	78
Figure 4. Quantification of pre-mixed powder composition patterns in experiment.....	80
Figure 5. The powder distribution in simulation result and ten sections	82
Figure 6. The simulated powder distribution results in ten sections.....	83
Figure 7. Powder distribution in (a). section1 and (b). section3 at different moments. ...	84
Figure 8. Simulation results and experimental validation	85

LIST OF TABLES

	Page
PAPER I	
Table 1. Ti6Al4V and TiB2 particle properties	12
Table 2. Sieve analysis of pure Cu powder.....	16
Table 3. Sieve analysis of 4047 Al powder	17
Table 4. The operating parameters in the experiments	21
PAPER II	
Table 1. The operating parameters in the modeling	44
PAPER III	
Table 1. The operating parameters in the modeling	62
PAPER IV	
Table 1. Sieve analysis of pure Cu powder.....	77
Table 2. Sieve analysis of 4047 Al powder	77
Table 3. The operating parameters in experiment and modeling.....	80

SECTION

1. INTRODUCTION

1.1. BACKGROUND

In order to satisfy increasing requirements from customers on material's diversified functions and applications, customized materials are garnering more and more attention because they can be fabricated to serve specific and tailored applications. Customized materials can be tailored to satisfy various property or functionality requirements as the usage needs and working environments demand. To fabricate such customized materials, Laser 3D printing, also called as Laser Metal Deposition (LMD), can be an effective processing technique. Using which, customized compositions varying across the volume of the part could be achieved. During the part's fabrication, the required custom composition can be attained by melting pre-mixed powders. The pre-mixed powders possess particular composition ratios to satisfy the usage requirement. Figure 1.1 is a schematic illustration depicting the process of fabricating customized material by LMD.

Depending on the composition requirements, several sorts of alloy or metal elemental powders are weighed. The weight percentages (wt.%) or volume percentages (vol.%) should meet the required chemical composition ratio for fabricating the customized materials. Then, all the weighed powders are blended sufficiently employing appropriate mixing equipment. This blended powder is then used as the powder feedstock during LMD process. A beneficial merit of pre-mixed powder is flexibility. Operators can produce powder feedstocks with any chemical composition ratio, and adjust the composition of

powder efficiently. Additionally, because pre-mixed powder is from mixing some basic alloy or elemental powder, it is better in saving manufacturing cost.

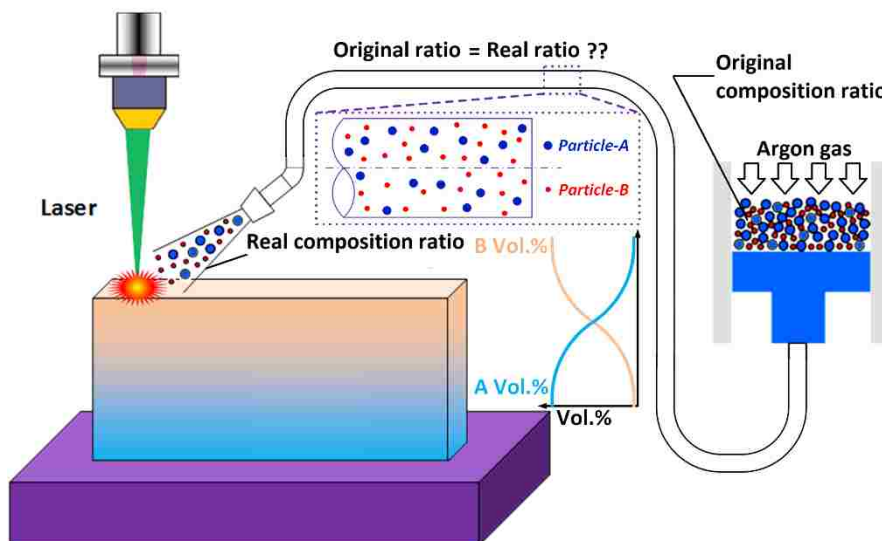


Figure 1.1. Customized material manufactured by Laser metal deposition.

However, the pre-mixed powder is not a perfect powder supply. As shown in Figure 1, inert gas flow (argon) is used to drive the powders along the powder feeder pipe, into the melt pool through the nozzle. Since the particles in the powder mixture have different densities and sizes, under the same argon gas flow the movement of powders will not be uniform in powder feeder pipe. Lighter and smaller particles could move faster while heavier and bigger particles could lag behind. This kind of pre-mixed powder separation may cause the deviation from the original composition ratio. In customized material, the material composition ratio in any different area is required strictly. Non-uniform powder mixture movements will skew the composition ratio, and reduce the material performance. This composition ratio deviation of pre-mixed powder is becoming a critical issue in

fabricating customized material using LMD. Hence, investigation on pre-mixed powder flow in powder feeder pipe is greatly necessary.

1.2. RESEARCH OBJECTIVES

The main objective of this research is to develop the key technologies for investigating pre-mixed powder flow in LMD process, since supplied pre-mixed powder directly affects the deposited composition, which is an important factor in guaranteeing customized material performance. Four research tasks are carefully studied to achieve this overall objective.

Specifically, the research task 1 answers the following question: How to observe the pre-mixed powder separation with experimental method? How to design the experiment since the observation of a great amounts of particles is very complicated. By mixing two kinds of powders (Cu and 4047 Al) with same volume percentages, and then delivered by uniform argon gas flow, the separation of pre-mixed powder in powder feeder pipe will be effectively observed. The difference of volume percentages in real powder mixture and original powder mixture will be compared. The experimental observation result will be utilized to validate the modeling simulation result of pre-mixed powder flows.

Research task 2 introduces a powerful numerical model which will be able to simulate the pre-mixed powder flow behaviors in powder feeder pipe. Powder feeding process in LMD is a standard fluid-particle system, which is composed of argon gas flow and metal powder. An effective modeling methodology to analyze the above fluid-particle system is a coupled Computational Fluid Dynamics method and Discrete Element Method (CFD-DEM), which has sufficient consideration of particle-particle collisions and fluid-

particle interactions. The DEM is Lagrangian method, in which all particles in the computational domain are tracked by explicitly to calculate the particle trajectories. The DEM method is capable of solving the contact forces that generated by the particles collision, which is modelled by the Spring collision law. The CFD method is employed to simulate the gas fluid-particle interaction, particle's dynamic behavior in argon gas flow, especially deeply understand the pre-mixed powder dynamic behavior. A CFD model mainly includes three types of equations: continuity equation of mass; momentum conservation equations, and k- ϵ kinetic energy equations.

With the proposed CFD-DEM model, research Task 3 studies pre-mixed powder's separation phenomenon in feeding process, and the effects of argon gas flow rate on the separation results. The processing parameters in the modeling simulation will be same with the experimental set-up. Therefore, the modeling results will be validated using the experimental analysis results. Compared to the experiment, modeling can also provide much more details in powder mixture feeding process, which are helpful explanation for the pre-mixed powder separation. In addition, three different argon gas flow rates will be utilized in powder flow models to investigate the argon gas flow rate's effect on separation results.

Research Task 5 introduces a novel particle size optimization idea as the solution to eliminate the powder separation and reduce the composition deviation. Through optimizing particle size, the acceleration of particles can be uniform or close to uniform, so that the original mixing composition can be maintained. The modeling results will be validated by the experimental analysis results. It can be clearly observed that the powder separation will be effectively controlled in both modeling and experimental results.

1.3. ORGANIZATION OF DISSERTATION

In this dissertation, there are four major developments been presented and been organized in the way. Paper I focuses on experimental study of pre-mixed powder separation in powder feeding process, which provides reliable experimental data, and can also be used to furtherly validate the proposed modeling results. Paper II mimics the powder mixture separation in powder feeder pipe with a comprehensive CFD-DEM model. A lot of details of pre-mixed powder flow behaviors in feeding process are simulated. The simulation results are then validated by the experimental results. Paper III investigates the effect of argon gas flow rate on the pre-mixed powder's separation in feeding process. Three different argon gas flow rates are selected and input to the CFD-DEM model. The different separation results are simulated then compared with experiment. Paper IV introduces a novel solution to eliminate the powder separation and reduce the composition deviation. The basic idea is to optimize the particle size to uniform the particle's acceleration. With this solution, the original mixing composition can be maintained, so that the composition deviation in deposited material can be effectively controlled.

PAPER**I. INVESTIGATION AND ELIMINATING POWDER SEPARATION IN PRE-MIXED POWDER SUPPLY FOR LASER METAL DEPOSITION**

Wei Li, Sreekar Karnati, Yunlu Zhang, and Frank Liou

Department of Mechanical and Aerospace Engineering

Missouri University of Science and Technology, Rolla, Missouri 65409, U.S.A.

ABSTRACT

Laser Metal Deposition (LMD) is an effective process to fabricate customized material compositions using pre-mixed powders. The deposited material composition is expected to be similar or same as supplied powder mixture. The current investigation is aimed at optimizing and setting up powder feed capable of producing consistent composition ratio in the output material using LMD process. Through experimental investigation the authors identified an important phenomenon: separation in powder mixture during flow from feeder to melt pool. Such separation can cause severe composition deviation in deposited material. This paper introduces a novel particle size optimization method as the solution to eliminate the powder separation. Two types of experiments were done in this study. First, pure Cu and 4047 Al powders were mixed with equal volume percentages (50% to 50%), and were transported from the powder feeder to the deposition site. The flow out of the feed tube was captured and preserved in an epoxy resin coating. The volume percentage of each type of powder was plotted by quantifying the distribution of different particles in the pattern. Clear powder separation and

consequently composition deviation was found in the first experiment result. During the second experiment, powder mixtures with the same volume percentage composition was transported and captured. However, the particle size distributions of Al4047 and Cu were optimized to equalize the particle acceleration during transportation in the feed tube. By optimizing powder size to equalize acceleration the powder separation was observed to be effectively eliminated. The composition deviation was also significantly reduced. The results from this study are pathbreaking contributions in the research of customized material fabrication with pre-mixed powder in LMD process.

1. INTRODUCTION

Customized materials are garnering more and more attention because they can be fabricated to serve specific and tailored applications. Customized materials can be tailored to satisfy various property or functionality requirements as the usage needs and working environments demand. To fabricate such customized materials, Laser Metal Deposition (LMD) can be an effective processing technique. Using which, customized compositions varying across the volume of the part could be achieved. During the part's fabrication, the required custom composition can be attained by melting pre-mixed powders. The pre-mixed powders possess particular composition ratios to satisfy the usage requirement. Figure1 is a schematic illustration depicting the process of fabricating customized material by LMD. Carroll and Otis [1] fabricated a customized material with functionally graded composition change from SS 304L to Inconel 625 by laser deposition process with pre-mixed powder as the feedstock. Planned variation in material properties across part's volume can be attained from gradual changes in the composition to meet the design

requirements. Li and Liou [2] demonstrated similar feasibility by fabricating a novel customized structure which successfully joined stainless steel and titanium alloy by means of laser deposition process with elemental powder feedstocks. Schwendner and Banerjee [3] used laser metal deposition process to deposit Ti–10%Cr alloy and Ti–10%Nb alloys with pre-mixed Ti-Cr and Ti-Nb powders. Banerjee and Collins [4] employed LMD with pre-mixed Ti-6Al-4V and elemental boron powders to deposit one customized alloy, Ti–6Al–4V–TiB, which combined the high strength and stiffness of the borides with the toughness and damage tolerance of a Ti-alloy.

The critical factor in fabricating customized material by LMD is the multi-composition powder feedstocks. Based on existing powder processing techniques, powder-mixing nozzle, pre-alloyed powder and pre-mixed powder are three main techniques to provide multi-composition powder. The powder-mixing nozzle employs a chamber to mix multiple powders to achieve multi-composition additive manufacturing [5]. This kind of nozzle is useful in fabricating customized material, but the complexity of nozzle increased the manufacturing cost. The powder mixing chamber Pre-alloyed powder feedstocks can deliver precise chemical composition, as the composition of powder particles is homogenous. Unlike pre-alloyed powder, there are limitations to the usage of pre-alloyed powder. First of all, customized materials strictly require the chemical compositions distribution in the whole structure. Pre-alloyed powder has the fixed chemical composition and cannot change anymore. Acquiring pre-alloyed powder with compositions similar to user requirements can be extremely difficult and expensive. If the pre-alloy powder cannot meet the composition need, it will become useless and new powder has to be sought for. Besides, the price of pre-alloyed powder is often expensive, so it is not good choice to

control the manufacturing cost. Owing to the above reasons, pre-mixed powder is preferred choice. The preparation of pre-mixed powder is very easy. According to the composition requirements, several kinds of alloy or metal elemental powders are weighed. The weight percentages (wt.%) or volume percentages (vol.%) should match the required chemical composition ratio needed for fabricating the customized materials. Then, all the weighed powders are blended adequately using appropriate mixing equipment. This blended powder is then used as the powder feedstock during LMD process. One of the valuable merits of pre-mixed powder is flexibility. Operators can produce powder feedstocks with any chemical composition ratio, and adjust the composition of powder efficiently. In addition, because pre-mixed powder is from mixing some basic alloy or elemental powder, it is better in saving manufacturing cost than pre-alloyed powders.

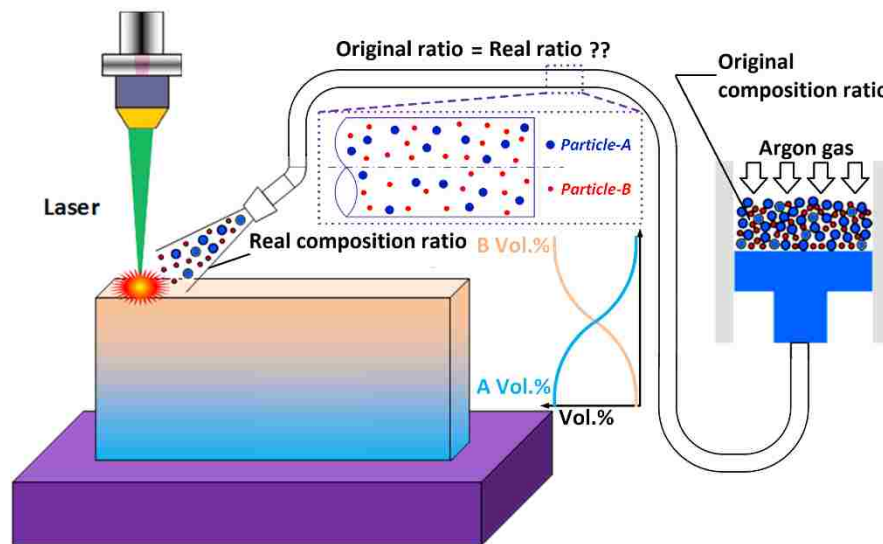


Figure 1. Schematic illustration of fabricating customized material by LMD.

However, the pre-mixed powder is not a perfect powder supply. As shown in Figure 1, the pre-mixed powders are fed through powder feeder during the process of LMD. Inert

gas flow (argon) is used to drive the powders along the powder feeder pipe, into the melt pool through the nozzle. Since the particles in the powder mixture have different densities and sizes, under the same argon gas flow the movement of powders will not be uniform in powder feeder pipe. Lighter and smaller particles could move faster while heavier and bigger particles could lag behind. This kind of particle flow dynamics may cause the deviation from the original composition ratio. In customized material, the material composition ratio in any different area is required strictly. Non-uniform powder mixture movements will skew the composition ratio, and reduce the material performance. This composition ratio deviation of pre-mixed powder is becoming a critical issue in fabricating customized material through LMD.

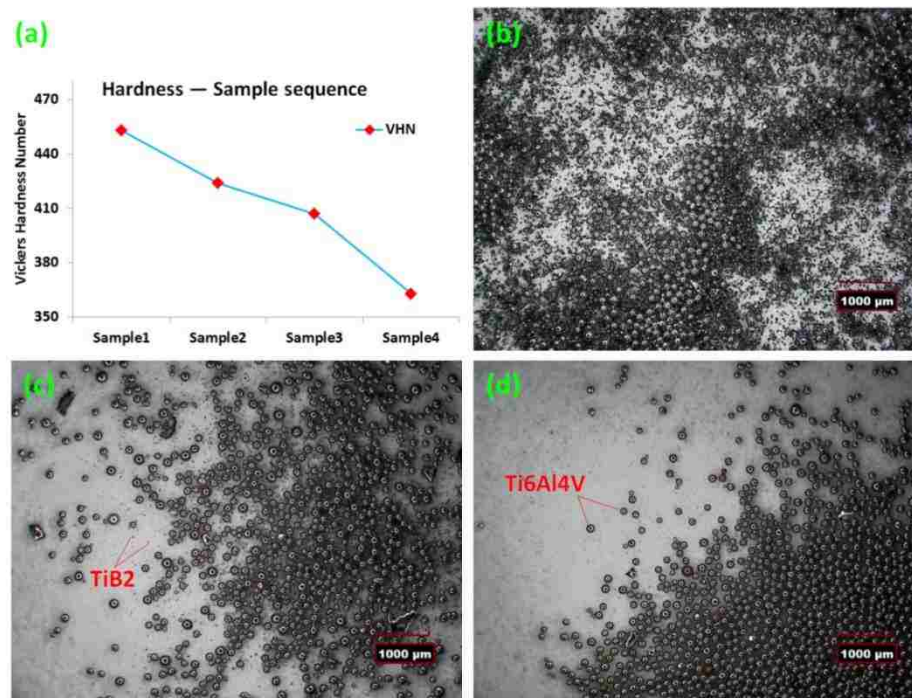


Figure 2. (a). VHN of four samples in sequence; (b). fresh mixed powders; (c). remaining mixed powders after prior two depositions; (d). remaining mixed powders after all the four depositions.

Figure 2. shows a research work done by authors before in fabricating a customized material of Ti6Al4V and TiB2. This research results provided a real example in which the non-uniform pre-mixed powder flow caused the deviation of customized material property. Ti6Al4V was used as substrate. Pre-mixed Ti6Al4V and TiB2 powders were prepared with designed wt.% ratio (Ti6Al4V:TiB2= 30:1). The density and particle size of two types of powder were described in Table.1. Both kinds of powder had close densities, but TiB2 particle size was much smaller than Ti6Al4V particle. Introducing of TiB2 can improve the modulus and strength of Ti6Al4V alloy [6]. This improvement can be observed through the Vickers Hardness Number (VHN). VHN of Ti6Al4V deposited with TiB2 should be greater than the VHN of regular Ti6Al4V. Four thin wall samples were fabricated in sequence by LMD process to investigate the VHN's repeatability through employing same powder mixing design and same processing parameters. Center points of four samples were selected as Vickers hardness test points. VHN comparison of four samples in sequence is shown in Figure 2a. From sample 1 to sample 4, VHN is observed as decreasing from 453 to 363. This result indicates the hardness of samples were not repetitive although the same pre-mixed powder and identical processing parameters were employed. Introducing TiB2 can enhance the hardness of Ti6Al4V because TiB2 is one type of ceramics with super high hardness. Decreasing VHNs of four samples indicates that consumed TiB2 powder reduced in sequence from sample 1 to sample 4. This deduction was also demonstrated by the optical microscopy images of mixed Ti6Al4V and TiB2 powders in Figure 2b-2d. Figure 2b shows the fresh mixed powders. Ti6Al4V particle is in the form of spherical ball with the mean diameter of 127 μm . TiB2 particle is one type of ceramics with irregular shape. TiB2 particle mean size is 26 μm which is much less than Ti6Al4V particle. In

Figure 2b, a lot of both particles can be observed clearly. Figure 2c shows the mixed powders after depositing first two samples and before 3rd deposition. It is easy to find that the amount of TiB₂ reduced sharply comparing with the amount in fresh mixed powders. Figure 2d. shows the mixed powders after all of four depositions. Almost no TiB₂ particle was observed and only Ti6Al4V particle were left. Through comparing the optical microscopy images of mixed powder, the composition ratio of powders did not keep designed ratio in the process of LMD. This kind of inaccurate composition ratio of pre-mixed powders is becoming a critical issue in process of fabricating functional material through LMD. Therefore, an effective solution for this issue is urgently needed.

Table.1. Ti6Al4V and TiB₂ particle properties

Particle	Density	Mean size
Ti6Al4V	4.43 g/cm ³	127 μm
TiB ₂	4.52 g/cm ³	26 μm

So far, there was no study focused on pre-mixed powders' dynamic behavior in LMD. Some of the previous research efforts on the powder flow were limited to identical material instead of mixed powders. Pan and Liou [7] studied gravity-driven metal powder flow in coaxial nozzle for laser-aided direct metal deposition process with the H13 tool steel powder. Pan and Liou also [8] also investigated the metallic powder flow in a coaxial nozzle for laser aided deposition process through numerical simulation method. Tan et.al [9] developed a photographic system for the titanium powder feeding process of laser solid forming in which high speed camera, particle speed and powder flow concentration behaviors were described based on the powder flow images. Pinkerton and Li [10] studied

the impact of powder feeder nozzle dimensions on powder flow rate. In their study, stainless steel 316L powder was used to analyze the behavior of the axial powder stream concentration from a coaxial laser cladding nozzle. Wen et.al [11] presented a comprehensive modeling method to predict the whole process of coaxial powder flow including the Stellite-6 particle stream flow in and after the powder feeder nozzle, and laser-particle interaction process. More attentions were paid on analyzing the powder stream behavior through both numerical and experimental methods, but the powder particles in any of these studies were the same material.

A study to investigate the pre-mixed powder flow in LMD process is lacking, so the purpose of this paper is to fill in this gap since supplied pre-mixed powder directly affects the deposited composition, which is an important factor in guaranteeing customized material performance. In this paper, experimental method was employed to present an important phenomenon: powder separation in blown powder mixture flow, which can cause severe composition deviation in deposited material. This paper also introduced a novel particle size optimization method as solution to eliminate the powder separation and reduce the composition deviation. Pre-mixed pure Cu and 4047 Al powders were used to do two experiments. The first experiment result disclosed powder separation. By optimizing the particle size in two types of powder, the powder separation was effectively solved in the second experiment result.

2. PARTICLE ACCELERATION ANALYSIS IN ARGON GAS FLOW

During the process of LMD, powder is transported through powder feeder pipe by argon gas, to the melt pool. Particle's dynamic behavior in argon gas flow is a complicated

problem to model. It is a two-phase problem called gas-particle flow. To deeply understand the pre-mixed powder flow dynamic behavior in powder feeder pipe, it is necessary to review the fundamental theories of particle acceleration in gas-particle flow. Figure 3 schematically illustrates the two primary driving forces for particle acceleration in the gas-particle flow. One is the fluid force, F_a , from the gas flow, while the other is particle gravity G . When the particles are moving, particle-particle collisions also occur. However, since the particle is a rare phase in gas-particle flow, and the powder feed rate is much less than the gas flow rate, the collision of particle-particle is negligible [11, 12].

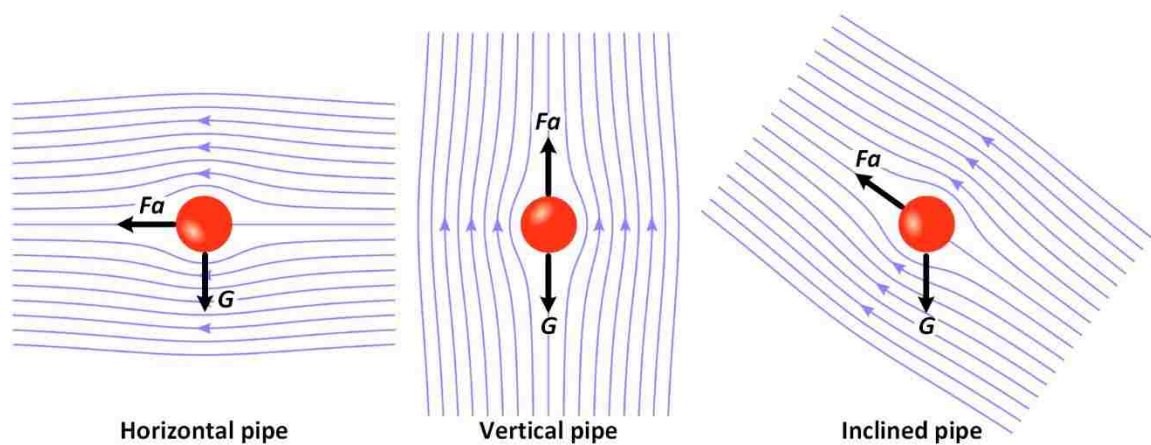


Figure 3. Two primary driving forces for particle.

The gas-particle flow problem involving the trajectory of a dispersed particle phase is solved by integrating the force balance on the particle in a Lagrangian reference frame.

The dynamic governing equations for each particle are written as follows [11].

$$\frac{d\vec{x}}{dt} = \mathbf{u}_p \quad (1)$$

$$\frac{d\mathbf{u}_p}{dt} = \frac{18\mu}{\rho_p d_p^2} \frac{C_D Re}{24} (\mathbf{u} - \mathbf{u}_p) + \frac{g(\rho_p - \rho)}{\rho_p} \quad (2)$$

Where u_p , ρ_p , and d_p are the velocity, density, and diameter of particle, respectively. Eqn. (2) indicates that the particles are basically driven by the forces of gas flow drag and gravity. C_D is the drag coefficient which is dimensionless quantity. Re is Reynolds number and μ is the viscosity of argon gas flow. The particle shape in this study is limited to spherical particle. For spherical particles, the drag coefficient can be taken from:

$$C_D = a_1 + \frac{a_2}{Re} + \frac{a_3}{Re^2} \quad (3)$$

Where a_1 , a_2 , and a_3 are constants that apply over several ranges of Re given by Morsi and Alexander [13]. The constants, a_i are defined as follows:

$$a_1, a_2, a_3 = \begin{cases} 0, 24, 0; & 0 < Re < 0.1 \\ 3.690, 22.73, 0.0903; & 0.1 < Re < 1 \\ 1.222, 29.1667, -3.8889; & 1 < Re < 10 \\ 0.6167, 46.50, -116.67; & 10 < Re < 100 \\ 0.3644, 98.33, -2778; & 100 < Re < 1000 \\ 0.357, 148.62, -47500; & 1000 < Re < 5000 \\ 0.46, -490.546, 578700; & 5000 < Re < 10000 \\ 0.5191, -1662.5, 5416700; & Re > 10000 \end{cases} \quad (4)$$

The Reynolds number of nozzle in laser metal powder deposition was tested as 7400 by Pan and Liou [7], which was used to calculate the drag coefficient C_D . By substituting the constants a_i in Eqn.4 to Eqn.3, the C_D was approximately estimated as 0.40.

3. EXPERIMENT PROCEDURE

To capture the result of the dynamic behavior of pre-mixed powder flow through powder feeder pipe and out of nozzle, pure Cu powder and 4047 Al powder were used in this research. The powder supplier is Atlantic Equipment Engineers. There are two reasons

behind choosing these two powders. Firstly, Cu particles are red or close to red, while 4047 Al is of gray color. The color difference makes it easy to differentiate between these two particles in the experiments. Secondly, the density of Cu particle is 8.94 g/cm³, while 4047 Al's density is only 2.6 g/cm³. The density of Cu is approximately three times that of 4047 Al density. According to Eqn. (2), particle acceleration is inversely proportional to particle density. Significant difference in density is expected to cause significant difference in particle acceleration. Therefore, the separation of pre-mixed powder is expected to be easy to observe.

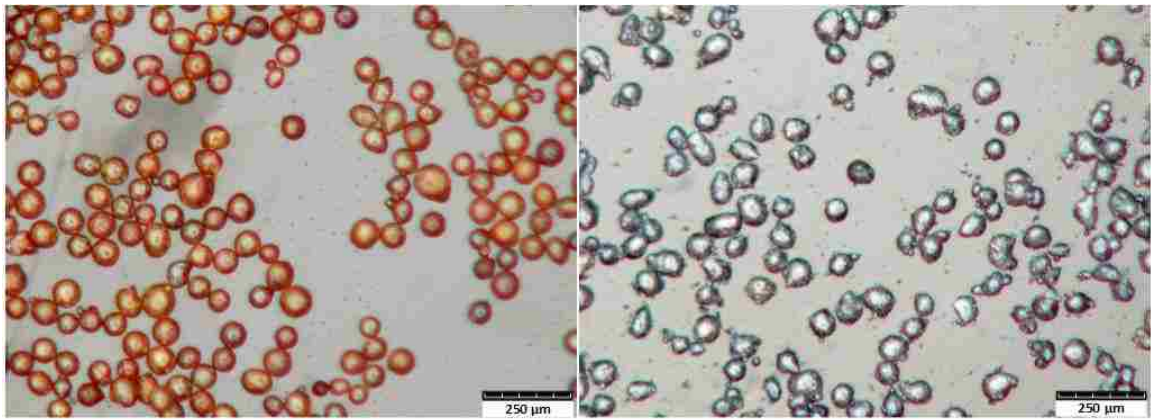
Figure 4. depicts the two types of powder particles through optical microscope images. The particle size distributions of the two types of powder obtained by sieve analysis are listed in Table.2 and Table.3. For pure Cu powder, most of the particles were observed to be spherical in shape. More than 80% of the particles had diameters in the range of 45-106 μm . In addition to this, 3.7% Cu particles diameters are 106-125 μm . The remaining Cu particles diameters are in the range of 125-212 μm . Most of the 4047 Al particles are spherical or close to spherical shape. Close to 30% particles ranged between diameters of 45 to 75 μm . More than 40% particles had diameters in the range of 75 to 106 μm . About 20% of particles had diameters in the range of 106 to 125 μm . 5% particles diameters are 125-150 μm . Some less amount of particles are bigger than 150 μm .

Table.2. Sieve analysis of pure Cu powder

Sieve type	+70 mesh	-70/+100 mesh	-100/+120 mesh	-120/+140 mesh	-140/+200 mesh	-200/+325 mesh
Size (μm)	>212	150-212	125-150	106-125	75-106	45-75
Percentage (%)	0.0	1.3	2.4	3.7	47.4	45.2

Table.3. Sieve analysis of 4047 Al powder

Sieve type	+70 mesh	-70/+100 mesh	-100/+120 mesh	-120/+140 mesh	-140/+200 mesh	-200/+325 mesh
Size (μm)	>212	150-212	125-150	106-125	75-106	45-75
Percentage (%)	1.1	2.8	5.4	20.3	42.5	27.9



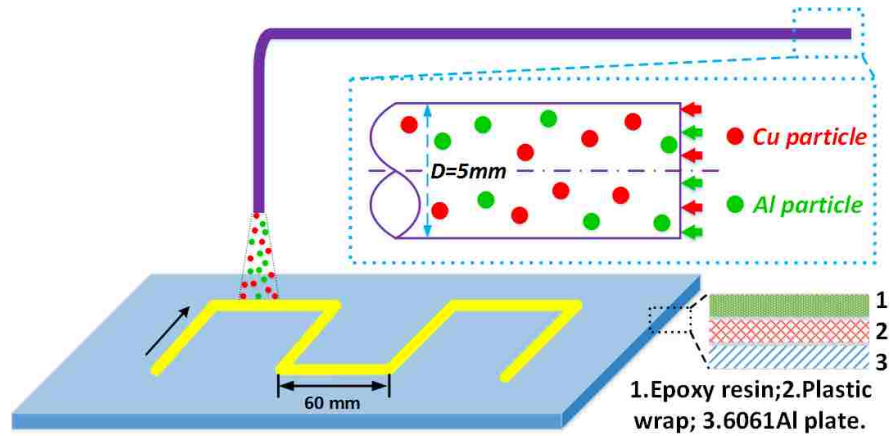
(a)

(b)

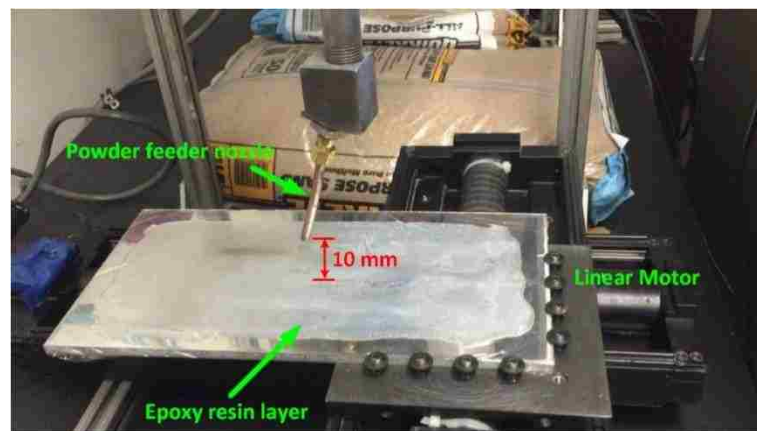
Figure 4. Optical microscopic images for: (a) Cu particles; and (b) 4047 Al particles.

The experimental setup is schematically shown in Figure 5. A commercial powder feeder (Bay State Surface Technologies, Inc, Model-1200) was used to supply pre-mixed powder. A polyurethane tube of 1.5m length and 5mm inner diameter, was used to deliver the pre-mixed powder. Two linear motors (AEROTECH, Inc, Model-100SMB2) were employed to generate moving path. A piece of 6061 Aluminum alloy plate, paved with sticky epoxy resin, was fixed on the motor table. The idea behind this experiment was to use the sticky epoxy resin layer to capture the pre-mixed 4047 Al and Cu powders as is while spraying out of the nozzle. The optical microscopy was used to observe the pre-mixed powder adhered on epoxy resin layer. The duration of this experiment was 25s. During this time, powder feeder nozzle was moved relative to the epoxy resin layer to

follow the specified path the letter “M”. After the epoxy resin was solidified, the adhered pre-mixed powder was contained in it.



(a)



(b)

Figure 5. Experiment set-up: (a) Schematic diagram; and (b) Work site

This research included two types experiments, whose design idea was based on the thinking of particle acceleration equation in Eqn.2. When particle is moving in powder feeder pipe driven by argon gas flow, there are two primary contributions for the particle acceleration. The first contribution is from argon gas dragging force, which carries particles along the powder feeder pipe to melt pool. The second contribution is from particle gravity,

which is always vertical down. For all the particles in pre-mixed powder, their acceleration gravity terms are equal or very close to equal, so the particle acceleration difference is mainly caused by various argon gas dragging force.

The particle acceleration Eqn.2 is a classic first order differential equation with variable of particle velocity u_p . In the process of laser metal powder deposition, each particle has such a differential equation for itself to describe its dynamic movement in powder feeder pipe. The second term on the right side can be simplified as gravitational acceleration g because particle density ρ_p is much greater than argon gas density ρ . The first term on the right side contains several coefficients including argon gas flow velocity u , drag coefficient C_D , argon gas density ρ , and the product of particle diameter d_p and density ρ_p . The coefficients u , C_D , and ρ are same for all the particles, but the product of density and diameter square $\rho_p d_p^2$ varies for different types of powders. In this study, the two particle densities ρ_{p_Cu} and ρ_{p_Al} , represent Cu particle density and 4047 Al particle density respectively. One ideal situation is, if Cu powder and 4047 Al powder have same density-diameter square products (in Eqn.5), then both type of particles will have uniform acceleration equations. The initial particle velocity is supposed as zero at powder feeder pipe orifice. Therefore, both types of particles will have the same or almost same velocity distribution and history, so that the separation of pre-mixed powder could be effectively eliminated.

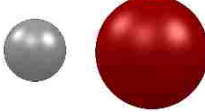

$$\rho_{p_Cu} d_{p_Cu}^2 = \rho_{p_Al} d_{p_Al}^2 \quad (5)$$

$$\frac{d_{p_Al}}{d_{p_Cu}} = \sqrt{\frac{\rho_{p_Cu}}{\rho_{p_Al}}} = \sqrt{\frac{8.94g/cm^3}{2.6g/cm^3}} = 1.854 \quad (6)$$

The Eqn.5 was rewritten in a new proportion format in Eqn.6, which explains an important criterion: if 4047 Al particle diameter is 1.854 times greater than Cu particle diameter, both type of particles will have same acceleration equations. Much closer the d_{p_Al}/d_{p_Cu} is to the ideal value, more effectively the powder mixture separation could be eliminated. Otherwise, if the d_{p_Al}/d_{p_Cu} much greater or less than the ideal value, the powder mixture will separate when flowing in powder feeder pipe since the mixed particles have different acceleration equations.

Based on above analysis, two experiments were designed. These two experiments were performed with same operating parameters, such as same volume percentage ratios, same argon gas flow rate, same moving speed of Aluminum plate, and same moving time. The only difference was the particle diameter. In the first experiment, 4047 Al powder with the particle diameter range (45-75 μm), and Cu powder with the particle diameter range (75-106 μm) were mixed in the volume percentage ratio of 50%:50%. Then in the second experiment, 4047 Al powder with the bigger particle diameter (75-106 μm), and Cu powder with the smaller particle diameter range (45-75 μm) were mixed in the same Vol.% ratio. Such experiment design came from the consideration of ideal particle diameter ratio value discussed above. The pre-mixed powder with smaller 4047 Al particle and bigger Cu particle was expected to separate easily because the particle diameter ratio d_{p_Al}/d_{p_Cu} was less than the ideal value. On the other hand, the pre-mixed powder in the second experiment had bigger 4047 Al particle and smaller Cu particle, so the particle diameter ratio d_{p_Al}/d_{p_Cu} was much closer to the ideal value than the first experiment. Under this situation, the pre-mixed powder separation would be eliminated due to the optimized particle diameter. The operating parameters in the experiments were shown in Table.4.

Table.4. The operating parameters in the experiments

	Experiment-1	Experiment-2(optimized)
Schematic particles (Gray-Al; Red-Cu)		
4047 Al particle diameter	45-75 μm	75-106 μm
Cu particle diameter	75-106 μm	45-75 μm
d_{p_Al}/d_{p_Cu}	0.667	1.5
Vol.% ratio	50%:50%	50%:50%
Argon gas flow rate	6 m/s	6 m/s
Al plate moving speed	1m/min	1m/min
Moving time	25 s	25 s

4. RESULTS AND DISCUSSION

After the sticky epoxy resin solidified on the plastic wrap, the pre-mixed particle pattern was observed. Figure 6 shows the two solidified epoxy resin layers containing powder patterns from the two experiments. This pattern was then sliced into 87 observation areas for the further analysis, including optical microscope observation and powder volume percentage quantification.

It was found that the first side in “M” shape was lost in the experiments. A rubber tube was used as powder feeder pipe, with the length of 2m. The CNC stage and powder feeder were activated simultaneously, so the powder had to flow through the powder feeder pipe at first, then sprayed out from nozzle. When the nozzle moving along the first section of “M”, the powder flow was right in the pipe. This is why the first side in “M” in the powder pattern was lost.



Figure 6. Two Pre-mixed powder patterns: (a) experiment-1; and (b) experiment-2.

4.1. ANALYSIS STEPS FOR THE EXPERIMENT RESULTS

In this study, three steps of analysis were performed to gather the experiment results. The first step was to observe the microscopic particle patterns along the powder capture path. 87 locations of size of 4mm by 3mm distributed at a uniform-interval along the central line of the powder path (shown in Figure 7) were observed. By observing the particle patterns in these zones, the pre-mixed powder flow's composition variation and the separation phenomenon can be clearly exposed. The next step was to quantify the distribution of different particles in the pattern. Basing the color difference of pre-mixed powder, the image processing software Image-J was used to mark 4047 Al particles and Cu particles in each observed zone, then count the particle numbers of the two powders. As the particle sizes were known from the sieve analysis, the volume of two powders in each observed zone were calculated by Eqn.7 and Eqn.8. Vol_{powder} indicates one type of powder's volume; $N_{particle}$ is the number of this type of particles in the observed zone. The particle diameter distribution was assumed as the Gaussian distribution. r_{mean} is the

mean radius, or the mathematical expectation value of the particle radius. Finally, in the third analysis step, the volume percentage of two powder's composition was plotted with all the data obtained from the 87 observed zones.

$$Vol_{powder} = N_{particle} \times \frac{4}{3} \pi r_{mean}^3 \quad (7)$$

$$Vol. \%_{powder1} = 100 \times \frac{Vol_{powder1}}{Vol_{powder1} + Vol_{powder2}} \quad (8)$$

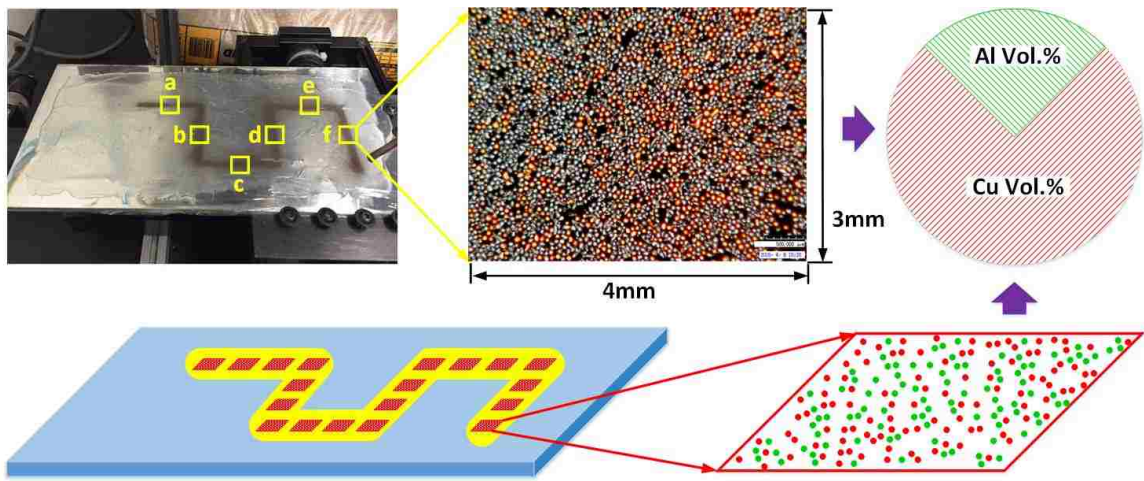


Figure 7. Observation of the experiment results

4.2. RESULTS OF EXPERIMENT

The pre-mixed powder particle pattern of experiment-1 was as shown in Figure 6a. The Hirox KH-8700 digital microscope was used to observe microscopic particle patterns following the path. Here six particle patterns locating in the middle points of the remaining six sides in “M” shape (Figure 6) were instanced, which were shown in Figure 8. Six optical micrographs effectively recorded powder patterns. The red color particles and gray color particles, respectively indicate the Cu particle and 4047 Al particles, were dispersively adhered to the epoxy resin layer. At the moment when particles just left the powder feeder

nozzle, the most particles were gray particles, which were 4047 Al. Some rare red Cu particles were scattering in the 4047 Al district. With the time increasing, more particles sprayed out from powder feeder nozzle, but the primary particles are still 4047 Al, which were found in Figure 8b, Figure 8c, and Figure 8d. When the particle pattern was close to the end of the “M” path, the red color became more and more remarkable (Figure 8e & Figure 8f). This phenomenon indicated that the volume percentage of Cu particle was increasing. From Figure 8a to Figure 8f, the six particle patterns show that the Pre-mixed powder did not keep the uniform composition. At the start and in the middle of the path, 4047 Al was the primary particle. Cu particle’s volume percentage gradually increased. This situation continued till the end of the path, where Cu particle had high volume percentage in the pattern. Since both powders started to transit simultaneously in powder feeder pipe inlet, but 4047 Al moved faster and exited from nozzle earlier than Cu particle, the separation of pre-mixed powder happened. The powder design was ruined by the separation of pre-mixed powder in their flow movement in the powder feeder pipe.

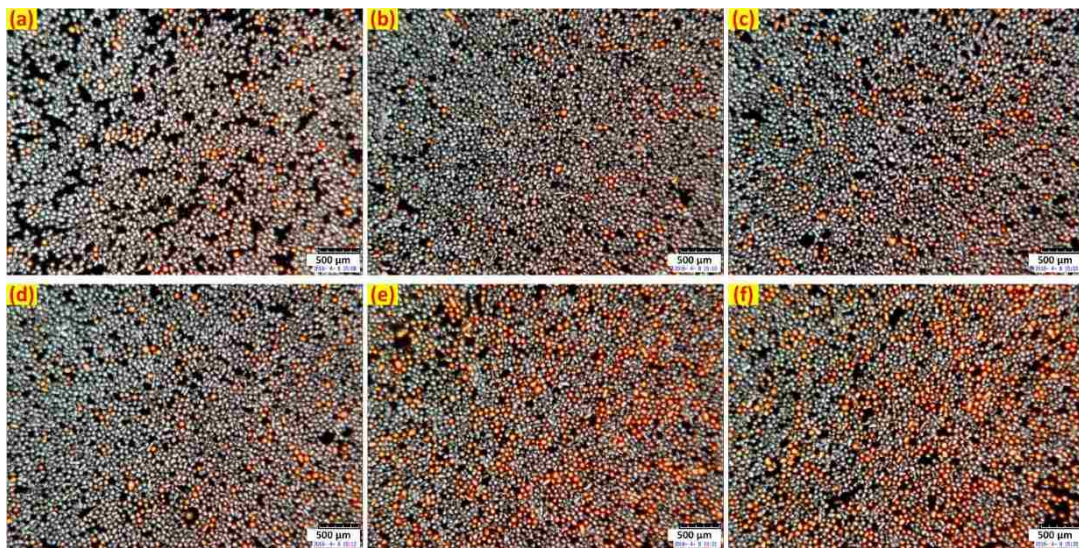


Figure 8. Six pre-mixed powder pattern zones in experiment-1.

The quantification of pre-mixed powder patterns was shown in Figure 9. 87 observed zones with the size of 4mm by 3mm distributed with uniform-interval along the central line of the powder path. The number of 4047 Al and Cu particles were counted with the assistance of image processing software Image-J. Then the volume of two powders in each observed zone can be calculated by Eqn.7 and Eqn.8. In Figure 9, blue color recorded the volume percentage of 4047 Al, while red color recorded the volume percentage of Cu. The time in the X-axis was used to indicate the moments when the particles in the relative observation zone reached the epoxy resin. From the pre-mixed powder flowing history, a clear tendency can be found. In the beginning stage (approximately 0s ~ 4s), no particle sprayed out from the nozzle, so the volume percentage of two powders was zero. Starting from the moment of 4s, a flow of powder mixture exited from the nozzle, in which 4047 Al was the primary particles, whose volume percentage reached to 93.25%. Some rare red Cu particles were found, whose volume percentage was 6.75%. With time increasing, more particles sprayed out from powder feeder nozzle, the primary particles are still 4047 Al, but whose volume percentage was decreasing gradually. In stark contrast, the volume percentage of Cu was gradually increasing. At the moment of 21s, Cu and 4047 Al had approximately same volume percentage. Then from the moment of 21s to the end, Cu powder volume percentage surpassed the 4047 Al powder volume percentage. Since both powders started to transit simultaneously from powder feeder pipe inlet, and 4047 Al particle had bigger acceleration than Cu particle according to the Eqn. 2, 4047 Al moved faster and exited from nozzle earlier than Cu particle. This is why Al powder volume percentage was greater than Cu powder. The powder volume percentage history in Figure 9 implied the pre-mixed powder separation since the two powders' volume percentage

were not uniform and kept changing, although they were designed as 50%:50%. The powder separation in their flow movement ruined the powder design and resulted in the severe deviation between original composition ratio and real composition ratio.

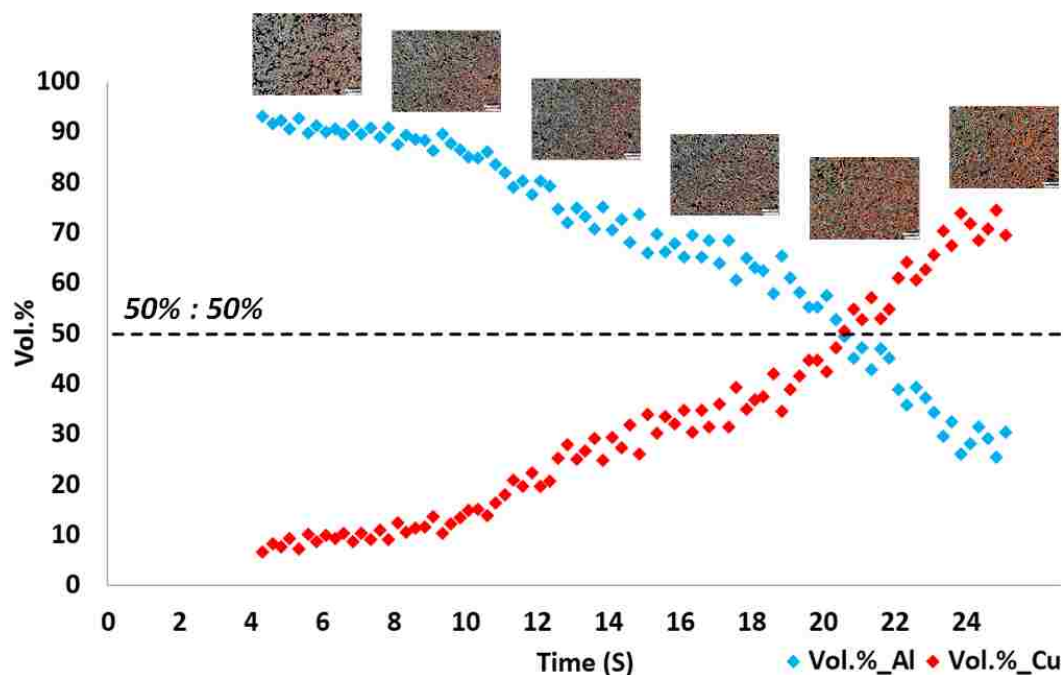


Figure 9. Pre-mixed powder volume percentage history in experiment-1.

Through selecting the particles with specific size to make the particle diameter ratio equal to or close to the ideal value in Eqn.6, the particle sizes were optimized in experiment-2. The pre-mixed powder particle pattern of experiment-2 was shown in Figure 6b. Six particle patterns, following the same location way as in the experiment-1, were instanced. Six optical micrographs effectively recorded pre-mixed powder particles in the experiment-2. From Figure 10a to Figure 10f, Cu particle and 4047 Al particles were dispersively adhered to the epoxy resin layer, and there were no obvious differences of color distribution. Comparing with the particle patterns in experiment-1 (Figure 8), the six

particle patterns in experiment-2 can keep approximately uniform. This phenomenon indicated that the pre-mixed powder separation can be effectively controlled by optimizing the particle size.

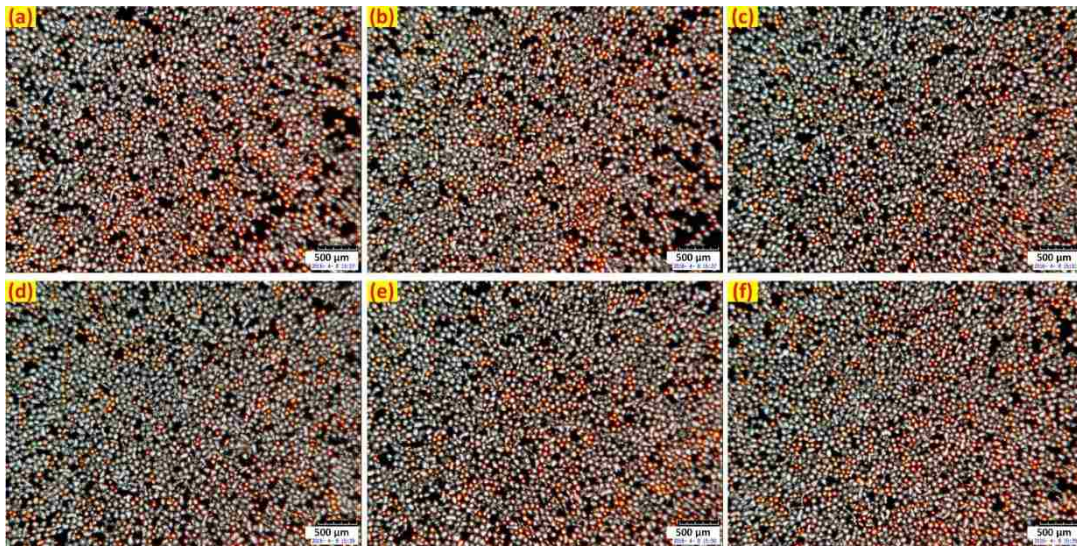


Figure 10. Six pre-mixed powder pattern zones in experiment-2.

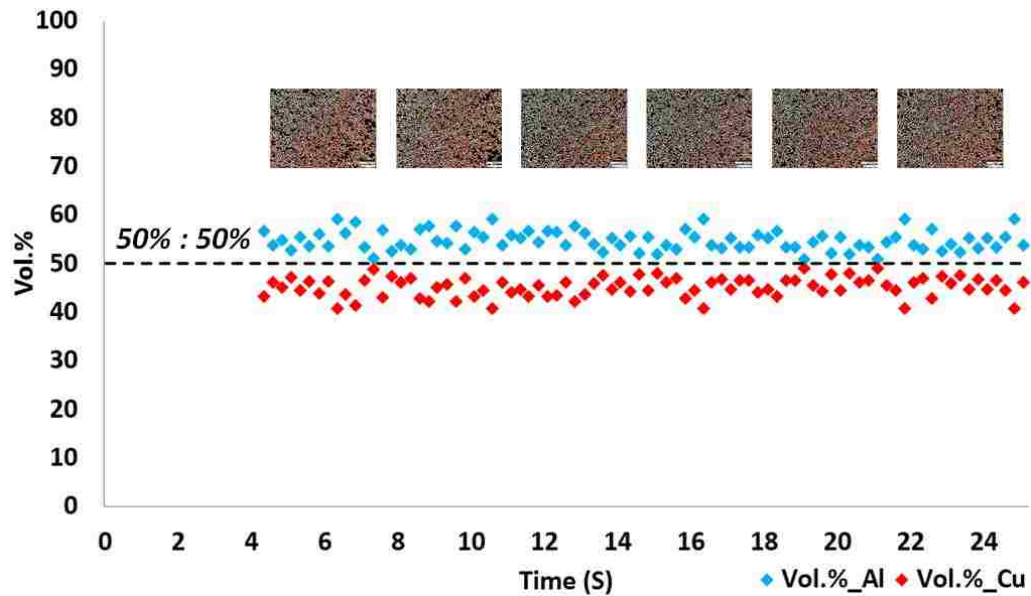


Figure 11. Pre-mixed powder volume percentage history in experiment-2.

The quantification of pre-mixed powder composition patterns in experiment-2 was shown in Figure 11. As same as in experiment-1, 87 observed zones with the size of 4mm by 3mm distributed with uniform-interval along the central line of the powder path. The number of 4047 Al and Cu particles were counted and them plotted. Blue color recorded the volume percentage of 4047 Al, while red color recorded the volume percentage of Cu. The time in the X-axis indicated the moments when the particles in the relative observation zone reached the epoxy resin. Therefore, the scatter diagram in Figure 11 can also be used as pre-mixed powder flow history diagram with optimized particles. By observing the optimized pre-mixed powder's composition distribution patterned in the epoxy resin coating, the powder flow had basically constant volume percentages, which were close to 50%:50%. Comparing with the results in experiment-1, the powder separation was effectively eliminated, so that the composition deviation was reduced.

5. CONCLUSION

This paper used an experimental method to present an important phenomenon: powder separation in blown pre-mixed powders flow. A novel particle size optimization method was introduced as solution to eliminate the powder separation to reduce the composition deviation. Some conclusions were summarized as follows:

In the pre-mixed powders, which have two types of powder with different densities, if the particle diameter ratio is equal to or close to an ideal value, all the particles will have the same acceleration when moving in powder feeder pipe. The ideal value is the square root of powder density ratio. Therefore, there will be very less powder separation. The

designed composition in pre-mixed powder can be maintained. The particle size optimization method is based on the particle acceleration theory. This optimization method has a limitation: the powder shape is limited in the spherical particle. For the irregular powder, the effect of the optimization is unknown.

Otherwise, if the particle diameter ratio is much greater or less than the ideal value, powder separation will happen in powder feeder pipe due to the different particle accelerations. It will cause the deviation between original composition and real composition. The designed composition in pre-mixed powder will be ruined.

REFERENCES

- [1] Carroll, B. E., Otis, R. A., Borgonia, J. P., Suh, J.-o., Dillon, R. P., Shapiro, A. A., Hofmann, D. C., Liu, Z.-K., and Beese, A. M., 2016, "Functionally graded material of 304L stainless steel and inconel 625 fabricated by directed energy deposition: Characterization and thermodynamic modeling," *Acta Materialia*, 108, pp. 46-54.
- [2] Li, W., Yan, L., Karnati, S., Liou, F., Newkirk, J., Taminger, K. M. B., and Seufzer, W. J., 2017, "Ti-Fe intermetallics analysis and control in joining titanium alloy and stainless steel by Laser Metal Deposition," *Journal of Materials Processing Technology*, 242, pp. 39-48.
- [3] Schwendner, K. I., Banerjee, R., Collins, P. C., Brice, C. A., and Fraser, H. L., 2001, "Direct laser deposition of alloys from elemental powder blends," *Scripta Materialia*, 45(10), pp. 1123-1129.
- [4] Banerjee, R., Collins, P., Genc, A., and Fraser, H., 2003, "Direct laser deposition of in situ Ti-6Al-4V-TiB composites," *Materials Science and Engineering: A*, 358(1), pp. 343-349.
- [5] Vaezi, M., Chianrabutra, S., Mellor, B., and Yang, S., 2013, "Multiple material additive manufacturing—Part 1: a review: this review paper covers a decade of research on multiple material additive manufacturing technologies which can produce complex geometry parts with different materials," *Virtual and Physical Prototyping*, 8(1), pp. 19-50.

- [6] Wang, F., Mei, J., and Wu, X., 2008, "Direct laser fabrication of Ti6Al4V/TiB," *Journal of materials processing technology*, 195(1), pp. 321-326.
- [7] Pan, H., Sparks, T., Thakar, Y. D., and Liou, F., 2006, "The investigation of gravity-driven metal powder flow in coaxial nozzle for laser-aided direct metal deposition process," *Journal of manufacturing science and engineering*, 128(2), pp. 541-553.
- [8] Pan, H., and Liou, F., 2005, "Numerical simulation of metallic powder flow in a coaxial nozzle for the laser aided deposition process," *Journal of Materials Processing Technology*, 168(2), pp. 230-244.
- [9] Tan, H., Zhang, F., Wen, R., Chen, J., and Huang, W., 2012, "Experiment study of powder flow feed behavior of laser solid forming," *Optics and Lasers in Engineering*, 50(3), pp. 391-398.
- [10] Pinkerton, A. J., and Li, L., 2002, "A verified model of the behaviour of the axial powder stream concentration from a coaxial laser cladding nozzle," *Proceedings of ICALEO*.
- [11] Wen, S., Shin, Y., Murthy, J., and Sojka, P., 2009, "Modeling of coaxial powder flow for the laser direct deposition process," *International Journal of Heat and Mass Transfer*, 52(25), pp. 5867-5877.
- [12] Zekovic, S., Dwivedi, R., and Kovacevic, R., 2007, "Numerical simulation and experimental investigation of gas-powder flow from radially symmetrical nozzles in laser-based direct metal deposition," *International Journal of Machine Tools and Manufacture*, 47(1), pp. 112-123.
- [13] Morsi, S., and Alexander, A., 1972, "An investigation of particle trajectories in two-phase flow systems," *Journal of Fluid mechanics*, 55(02), pp. 193-208.

II. NUMERICALLY SIMULATING THE SEPARATION OF PRE-MIXED POWDER FLOW SUPPLIED FOR LASER METAL DEPOSITION AND EXPERIMENTAL VALIDATION

Wei Li, Xinchang Zhang, Jingwei Zhang and Frank Liou

Department of Mechanical and Aerospace Engineering

Missouri University of Science and Technology, Rolla, Missouri 65409, U.S.A.

ABSTRACT

Pre-mixed powders are often used to fabricate functional graded materials or other customized materials with flexibly varying composition through Laser Metal Deposition (LMD) process. The varying composition is basically controlled by pre-mixed powders' composition with customized original blending ratio. The deposited material composition is expected to be similar or same as supplied powder mixture. However, during argon gas flow feeding powder process, because of complex gas dynamic interaction of particle and argon gas flow, the pre-mixed powder could experience separation, which can cause severe composition deviation in deposited material. The current investigation is aimed at modeling analysis of this important phenomenon: separation in powder mixture during flow from feeder to melt pool. This paper presents a comprehensive CFD-DEM model, which simulated the powder separation of pre-mixed powder supplied for LMD. By solving discrete particle force balance equations coupled with continuity equations and momentum equations for argon gas, the dynamic behavior of pre-mixed powder flow through feeder pipe and out of nozzle was simulated.

1. INTRODUCTION

Laser Metal Deposition (LMD) is a powerful manufacturing process to fabricate functional materials which can be customized to fulfill numerous property or functionality requirements as the utilization and working conditions needs. Within the part's fabricating process, the demanded functional composition can be gained by melting pre-mixed powders, which have specified composition ratios to satisfy the usage requirement[1]. Many researchers employed LMD process to manufacture the functional materials with customized designs, and have done a lot of material characterization and related analysis. Carroll and Otis [2] fabricated a customized material with functionally graded composition change from SS 304L to Inconel 625 by LMD process with pre-mixed powder as the feedstock. Designed variation in material properties throughout part's volume can be achieved from gradual changes in the composition to meet up with the design requirements. Schwendner and Banerjee [3] used LMD process to deposit Ti–10%Cr alloy and Ti–10%Nb alloys with pre-mixed Ti-Cr and Ti-Nb powders. Li and Liou [4-7] demonstrated similar feasibility by fabricating a novel customized structure which successfully joined stainless steel and titanium alloy by means of LMD process with elemental powder feedstocks. In addition, Li and Liou [8, 9] blended Fe-Cr-Ni elemental powders and then fabricated a new functional gradient alloy, in which the gradient volume change of Ni achieved a gradient composition change from primary ferrite to primary austenite. Yan and Chen [10-12] applied LMD process and mixed Ti, Al, V elemental powders to fabricate functional Titanium alloy and Ti-Al alloy, coupled with numerical simulation to analyze the cooling rate's effect on processing.

In the fabrication process, based on the composition requirements, several sorts of alloy or metal elemental powders are weighed. The weight percentages (wt.%) or volume percentages (vol.%) should meet the required chemical composition ratio for fabricating the functional materials. Then, all the weighed powders are blended sufficiently employing appropriate mixing equipment. This blended powder is then used as the powder feedstock during LMD process. A beneficial merit of pre-mixed powder is flexibility. Operators can produce powder feedstocks with any chemical composition ratio, and adjust the composition of powder efficiently. Additionally, because pre-mixed powder is from mixing some basic alloy or elemental powder, it is better in saving manufacturing cost. However, the pre-mixed powder is not a perfect powder supply. Inert gas flow (argon) is used to drive the powders along the powder feeder pipe, into the melt pool through the nozzle. Since the particles in the powder mixture have different densities and sizes, under the same argon gas flow the movement of powders will not be uniform in powder feeder pipe. Lighter and smaller particles could move faster while heavier and bigger particles could lag behind. This kind of pre-mixed powder separation may cause the deviation from the original composition ratio. In functional material, the material composition ratio in any different area is required strictly. Non-uniform powder mixture movements will skew the composition ratio, and reduce the material performance. This composition ratio deviation of pre-mixed powder is becoming a critical issue in fabricating functional material using LMD. Hence, investigation on pre-mixed powder flow in powder feeder pipe is greatly necessary.

However, there was no modeling or experimental study focused on pre-mixed powders' separation behavior in LMD. A few of the earlier research works on the powder

flow were narrowed to identical material rather than mixed powders. Pan and Liou [14] studied gravity-driven metal powder flow in coaxial nozzle for laser-aided direct metal deposition process with the H13 tool steel powder. By modeling analysis and experimental validation, the particle concentration is influenced significantly by nozzle geometries and argon gas velocity. Pan and Liou also [15] also investigated the metallic powder flow in a coaxial nozzle for laser aided deposition process through numerical simulation method. Tan et.al [16] developed a photographic system for the titanium powder feeding process of laser solid forming in which high speed camera, particle speed and powder flow concentration behaviors were described based on the powder flow images. Pinkerton and Li [17] studied the impact of powder feeder nozzle dimensions on powder flow rate. In their study, stainless steel 316L powder was used to analyze the behavior of the axial powder stream concentration from a coaxial laser cladding nozzle. Wen et.al [18] presented a comprehensive modeling method to predict the whole process of coaxial powder flow including the Stellite-6 particle stream flow in and after the powder feeder nozzle, and laser-particle interaction process. Extra efforts were dedicated on studying the powder stream behavior with the aid of both modeling and experimental methods, but the powder particles in any of these studies were the same material.

Since the study to analyze the blended powder separation in LMD process is lacking, the goal of this paper is to fill in this gap because supplied pre-mixed powder straightly affects the deposited composition, which is a crucial factor in ensuring customized material functionality. This study presents a comprehensive CFD-DEM model, which analyzed the powder separation in pre-mixed powder supplied for LMD process. By solving discrete particle force balance equations coupled with continuity equations and

momentum equations for argon gas, the dynamic behavior of pre-mixed powder flow through feeder pipe and out of nozzle was simulated. The simulation results were then validated by the experiment done by authors.

2. CFD-DEM MODELING METHODOLOGY

Powder is delivered by argon gas flow throughout the powder feeder pipe during the LMD. A typical fluid-particle system is constituted by both powder and argon gas flow. In this system, particle or granular material's motion is caused or driven by the fluid medium's flow motion and fluctuation. An encouraging modeling approach to investigate the above fluid-particle system is a coupled Computational Fluid Dynamics method and Discrete Element Method (CFD-DEM), which properly considers the interaction of fluid and particle [19].

The discrete element method (DEM) is appropriate to simulate granular matter (such as gravel, coal, beads of any material). The DEM is Lagrangian method, meaning that all particles in the computational domain are tracked by explicitly to solve the particle trajectories. The force balance for a particle i in its translational motion is expressed as follows:

$$m_i \frac{d\vec{v}}{dt} = F_{ij}^c + F_i^f + F_i^g \quad (1)$$

$$\frac{dx}{dt} = \vec{v} \quad (2)$$

where x denotes the translational displacement of the particle i . F_{ij}^c is the contact force acting on particle i by particle j or walls. F_i^f is the fluid-particle interaction force acting on particle i , which is the primarily drag force. F_i^g is the gravitational force.

The collision of particles causes the contact force, which can be calculated and analyzed using DEM model. The particle contact forces are determined by the deformation, which is measured as the overlap between pairs of spherical particles or between spherical particle and boundary [20]. Spring collision law was applied to model the contact force acting on particles due to particle-particle or particle-wall collisions. Eqn.3-7 explain how to use the linear spring collision law to calculate the contact forces. A unit vector \vec{e}_{12} is defined from particle 1 to particle 2, where x_1 and x_2 represent the position of particle 1 and particle 2, respectively. The overlap δ is defined in Eqn.4, which is less than zero during contact, where r_1 and r_2 represent the radii of particle 1 and particle 2, respectively. The force on particle 1 \vec{F}_1 is then calculated using a spring constant K that defined in Eqn.5, where D is the particle diameter, ρ is the particle mass density, v is the relative velocity between two colliding particles, and ε_D is the fraction of the diameter for allowable overlap. Then by Newton's third law, the contact force on particle 2 \vec{F}_2 is calculated through Eqn.7. Note that \vec{F}_1 is directed away from particle 2, because δ is negative for contact.

$$\vec{e}_{12} = \frac{x_2 - x_1}{\|x_2 - x_1\|} \quad (3)$$

$$\delta = \|x_2 - x_1\| - (r_2 + r_1) \quad (4)$$

$$K = \frac{\pi v^2}{3\varepsilon_D^2} D\rho \quad (5)$$

$$\vec{F}_1 = K\delta\vec{e}_{12} \quad (6)$$

$$\vec{F}_2 = -\vec{F}_1 \quad (7)$$

Argon gas flow transports powder through powder feeder pipe in the LMD process.

Particle's dynamic behavior in argon gas flow is a two-phase problem called gas-particle

flow. To deeply understand the pre-mixed powder dynamic behavior in powder feeder pipe, it is necessary to review the fundamental theories of particle acceleration in argon gas flow. Figure 1 schematically illustrates the two primary driving forces for particle acceleration. One is the gas fluid force, F_a , from the gas flow, while the other is particle gravity G [18].

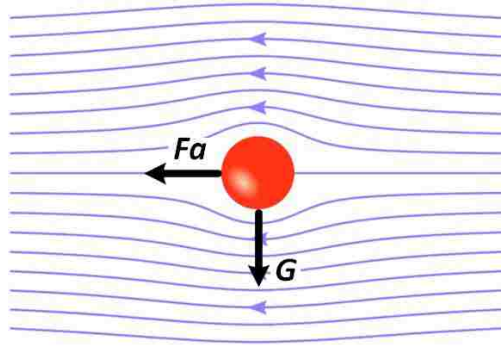


Figure 1. Two primary driving forces for particle.

The gas fluid-particle interaction problem involving the trajectory of a dispersed particle phase is solved by integrating the force balance on the particle in a Lagrangian reference frame. The dynamic governing equations for each particle are written as follows [18].

$$\frac{d\vec{x}}{dt} = u_p \quad (8)$$

$$\frac{du_p}{dt} = \frac{18\mu}{\rho_p d_p^2} \frac{C_D Re}{24} (u - u_p) + \frac{g(\rho_p - \rho)}{\rho_p} \quad (9)$$

Where u_p , ρ_p , and d_p are the velocity, density, and diameter of particle, respectively. Eqn. (9) indicates that the particles are basically driven by the integration of gas flow drag force and gravity. C_D is the drag coefficient which is dimensionless quantity. Re is Reynolds number and μ is the viscosity of argon gas flow.

For spherical particles, the drag coefficient can be taken from:

$$C_D = a_1 + \frac{a_2}{Re} + \frac{a_3}{Re^2} \quad (10)$$

Where a_1 , a_2 , and a_3 are constants that apply over several ranges of Re given by Morsi and Alexander [21]. The constants, a_i are defined as follows:

$$a_1, a_2, a_3 = \begin{cases} 0, 24, 0; & 0 < Re < 0.1 \\ 3.690, 22.73, 0.0903; & 0.1 < Re < 1 \\ 1.222, 29.1667, -3.8889; & 1 < Re < 10 \\ 0.6167, 46.50, -116.67; & 10 < Re < 100 \\ 0.3644, 98.33, -2778; & 100 < Re < 1000 \\ 0.357, 148.62, -47500; & 1000 < Re < 5000 \\ 0.46, -490.546, 578700; & 5000 < Re < 10000 \\ 0.5191, -1662.5, 5416700; & Re > 10000 \end{cases} \quad (11)$$

The Reynolds number of nozzle in laser metal powder deposition was tested as 7400 by Pan and Liou [14], which was used to calculate the drag coefficient C_D . By substituting the constants a_i in Eqn.11 to Eqn.10, the C_D was approximately estimated as 0.40.

Because of the gas fluid-particle interaction behavior, the argon gas flow in powder feeder pipe is characterized by the turbulence. A turbulence model was built to solve the dynamic fluid behavior of argon gas phase. The turbulence model includes three types of equations: continuity equation of mass; momentum conservation equations, and $k - \varepsilon$ kinetic energy equations. The governing equations are given as follows [18, 20, 22]:

Continuity equation of argon gas mass:

$$\frac{\partial(\rho u_j)}{\partial x_j} = 0 \quad (12)$$

where ρ is the density of argon gas, u_j is the velocity vector along the j th direction. Because of the axisymmetric calculation domain, u_j should be decomposed to axial

velocity vector u_x and radial velocity vector u_r . Therefore, the argon gas mass continuity conservation equation is deduced as:

$$\frac{\partial(\rho u_x)}{\partial x} + \frac{1}{r} \frac{\partial(r \rho u_r)}{\partial r} = 0 \quad (13)$$

Where x and r are the axial and radial coordinate, respectively.

The momentum conservation equation in the axial direction:

$$\begin{aligned} \frac{\partial(\rho u_x u_x)}{\partial x} + \frac{1}{r} \frac{\partial(r \rho u_r u_x)}{\partial r} = & -\frac{\partial p}{\partial x} + \frac{1}{r} \frac{\partial}{\partial x} \left[r \mu \left(2 \frac{\partial u_x}{\partial x} - \frac{2}{3} (\nabla \cdot \vec{u}) \right) \right] + \frac{1}{r} \frac{\partial}{\partial r} \left[r \mu \left(\frac{\partial u_x}{\partial r} + \frac{\partial u_r}{\partial x} \right) \right] \\ & + \phi_x \end{aligned} \quad (14)$$

The momentum conservation equation in the radial direction:

$$\begin{aligned} \frac{\partial(\rho u_x u_r)}{\partial x} + \frac{1}{r} \frac{\partial(r \rho u_r u_r)}{\partial r} = & -\frac{\partial p}{\partial r} + \frac{\partial}{\partial x} \left[\mu \left(\frac{\partial u_x}{\partial r} + \frac{\partial u_r}{\partial x} \right) \right] + \frac{1}{r} \frac{\partial}{\partial r} \left[r \mu \left(2 \frac{\partial u_r}{\partial r} - \frac{2}{3} (\nabla \cdot \vec{u}) \right) \right] \\ & - 2 \mu \frac{u_r}{r^2} + \frac{2}{3} \frac{\mu}{r} (\nabla \cdot \vec{u}) + \phi_r \end{aligned} \quad (15)$$

where ∇ is the Hamilton operator, μ is the effective dynamic viscosity of the continuous argon gas.

$$\nabla \cdot \vec{u} = \frac{\partial u_x}{\partial x} + \frac{\partial u_r}{\partial r} + \frac{u_r}{r} \quad (16)$$

In Eqns. (14) and (15), the source term ϕ_i ($i = x, r$) represents the coupled momentum transport from the particle phase:

$$\phi_i = \frac{1}{V_c} \sum_{j=1}^{n_c} \frac{3\mu C_D Re}{4\rho_p d_p^2} (u_{p,i} - u_i) \dot{m}_p^j \Delta t^j \quad (17)$$

where V_c is the volume of one cell C; \dot{m}_p^j is the particle mass rate for the j th trajectory passing through this cell; n_c is the total number of particle trajectories passing through the cell; Re and C_D are the Reynolds number and the drag coefficient of one particle; ρ_p , d_p ,

and $u_{p,i}$ are the density, diameter, and velocity in direction of one particle, respectively [18].

The turbulence flow in powder feeder pipe requires appropriate modeling procedure to describe the turbulent fluctuation effects on particle movements. The most popular turbulent model is the standard $k - \varepsilon$ model which is proposed by Launder and Spalding [23]. The turbulence behavior is described through introducing two additional variables: the turbulent kinetic energy k , and the viscous dissipation rate of turbulent kinetic energy ε . Serag-Eldin and Spalding [22] provided detailed description and expressions for these two variables. The standard $k - \varepsilon$ model is used to simulate the argon gas flow in powder feeder pipe.

Considering the axisymmetric calculation domain, the conservation of kinetic energy of turbulence is:

$$\frac{\partial(\rho u_x k)}{\partial x} + \frac{1}{r} \frac{\partial(r \rho u_r k)}{\partial r} = \frac{\partial}{\partial x} \left[\left(\mu_l + \frac{\mu_t}{\sigma_k} \right) \frac{\partial k}{\partial x} \right] + \frac{1}{r} \frac{\partial}{\partial r} \left[r \left(\mu_l + \frac{\mu_t}{\sigma_k} \right) \frac{\partial k}{\partial r} \right] + G_k - \rho \varepsilon \quad (18)$$

The conservation of the viscous dissipation rate of turbulent kinetic energy is:

$$\begin{aligned} \frac{\partial(\rho u_x \varepsilon)}{\partial x} + \frac{1}{r} \frac{\partial(r \rho u_r \varepsilon)}{\partial r} \\ = \frac{\partial}{\partial x} \left[\left(\mu_l + \frac{\mu_t}{\sigma_\varepsilon} \right) \frac{\partial \varepsilon}{\partial x} \right] + \frac{1}{r} \frac{\partial}{\partial r} \left[r \left(\mu_l + \frac{\mu_t}{\sigma_\varepsilon} \right) \frac{\partial \varepsilon}{\partial r} \right] + C_1 G_k \frac{\varepsilon}{k} - C_2 \rho \frac{\varepsilon^2}{k} \end{aligned} \quad (19)$$

$$\mu = \mu_l + \mu_t; \quad \mu_t = \rho C_\mu k^2 / \varepsilon \quad (20)$$

where μ_l and μ_t represent the laminar and turbulent viscosity. They are solved by the Eqn. (20). G_k is the rate of production of kinetic energy. The model constants have five constants C_1 , C_2 , C_μ , σ_k , and σ_ε , which have following default values [23]. These default values have been determined for fundamental turbulent flows including frequently encountered shear

flows like boundary layers, mixing layers and jets as well as for decaying isotropic grid turbulence [20].

$$C_1 = 1.44; C_2 = 1.92; C_\mu = 0.09; \sigma_k = 1.0; \sigma_\varepsilon = 1.30 \quad (21)$$

3. MODELING PREPARATION

A 3-dimensional calculation domain used in the CFD-DEM model is illustrated in Figure 2(a). The powder feeder pipe shape was designed like this to make the calculation domain close to the real experiment condition Figure 2(b). The direction of nozzle was leaning at 30 degree angle with the vertical pipe. The boundary condition of inlet was set as velocity inlet boundary, which was indicated with blue color. The velocities of argon gas flow and pre-mixed powder flow were applied at this boundary condition. Powder feeder pipe wall, which was indicated with magenta, was set as wall boundary condition. In computational fluid mechanics, wall means there is not any mass, flow, pressure passing through the wall. A calculation domain for powder spraying behavior was defined near the outlet nozzle of powder feeder pipe, whose boundary was indicated with black color. Outflow boundary condition was used surrounding the powder spraying domain. The outflow boundary is used to simulate the boundary condition where unknown outlet velocity and pressure happen but follow the developing process of fluid flow and conservation requirement.

The gas fluid–particle system discussed above is a complex two phase problem. In this study, the gas phase is treated as continuum, while the particle phase is simulated as a discrete phase that consists of two different particles dispersing in the continuous argon

gas phase. The fluid behavior of continuous gas phase is modeled by solving the continuity equations (Eqn.12, Eqn.13) and Navier–Stokes equations (Eqn.14, Eqn.15). The dispersed phase is solved by tracking a certain number of particles through the calculated domain. The trajectory of a discrete phase particle is solved by integrating the force balance on the particle, which is written in a Lagrangian reference frame [24]. The argon gas flow behavior in powder feeder pipe and near nozzle was simulated first by solving the turbulence model. Then the acquired argon gas flow field was used as the input for simulating the pre-mixed powder flow. The particle properties, including densities, size, shape, vol.% ratio, inlet velocity, were defined before calculation. Then powder flow field in the pipe and near the nozzle was simulated by coupling solving the interactions between the two phases and particle acceleration equations.

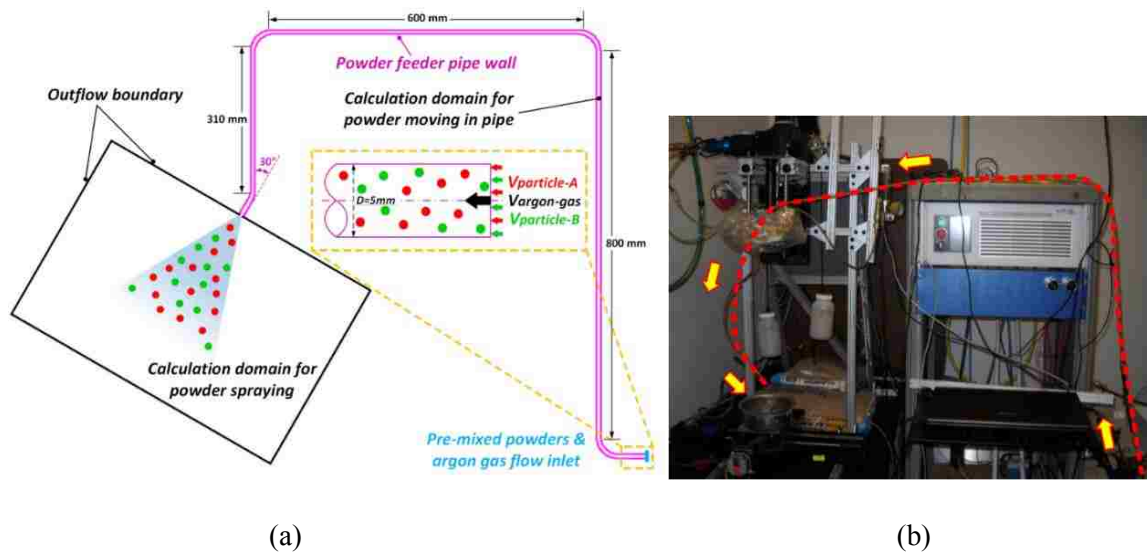
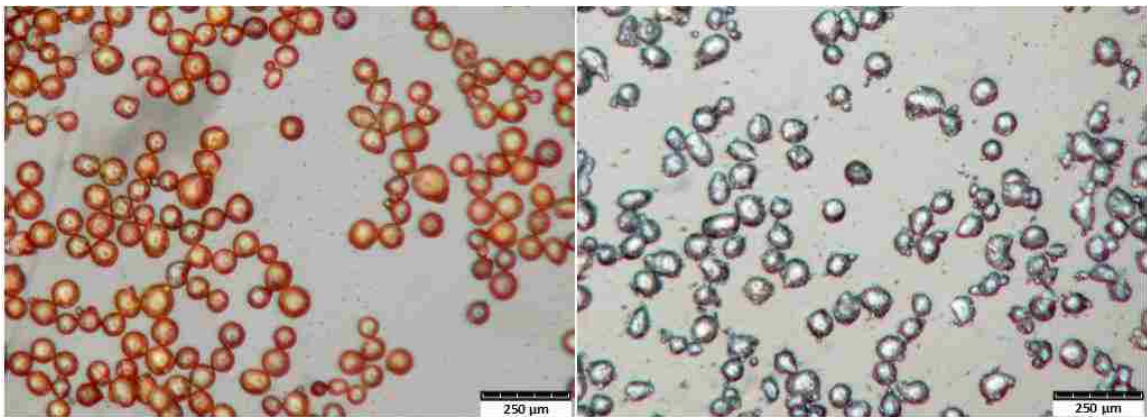


Figure 2. Modeling set-up: (a) calculation domain; (b) real situation in lab

Two types of powders were used in the experiment to validate the modeling result. Pure Cu powder and 4047 Al powder were supplied from Atlantic Equipment Engineers.

There were two reasons behind choosing these two powders. Firstly, Cu particles are red or close to red, while 4047 Al is of gray color. The color difference makes it easy to differentiate between these two particles in the experiments. Secondly, the density of Cu particle is 8.94 g/cm^3 , while 4047 Al's density is only 2.6 g/cm^3 . The density of Cu is approximately three times that of 4047 Al density. According to Eqn. (9), particle acceleration is inversely proportional to particle density. Significant difference in density is expected to cause significant difference in particle acceleration. Therefore, the separation of pre-mixed powder is expected to be easy to observe. Figure 3 depicts the two types of powder particles through optical microscope images. Both types of particles were observed to be spherical or close to be spherical in shape. After sieve analysis of both powder, the Cu powder with the particle size distribution of $75\text{-}106 \text{ }\mu\text{m}$, and the 4047 Al powder with the particle size distribution of $45\text{-}75 \text{ }\mu\text{m}$, were chosen for study.



(a)

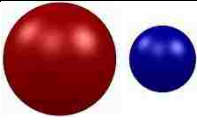
(b)

Figure 3. Optical microscopic images for: (a) Cu particles; and (b) 4047 Al particles

The operating parameters in the modeling calculation were shown in Table.1, which were same as the experiment[1] done before. 4047 Al powder with the particle diameter

range (45-75 μm), and Cu powder with the particle diameter range (75-106 μm) were mixed in the volume percentage ratio of 50%:50%. The argon gas flow rate was set as 6 m/s..

Table.1. The operating parameters in the modeling

Parameter	Value
Schematic particles (Blue-Al; Red-Cu)	
4047 Al particle diameter	45-75 μm
Cu particle diameter	75-106 μm
Vol.% ratio	50%:50%
Argon gas flow rate	6 m/s

4. SIMULATION RESULTS AND DISCUSSION

Figure 4 depicts pre-mixed powder distribution simulated by the CFD-DEM modeling. Blue color and red color were used to indicate the trajectories of 4047 Al particle and Cu particle respectively. Pre-mixed powder was supplied at the inlet of pipe under the condition of 6 m/s argon gas flow rate. Due to strong turbulence at the inlet, the pre-mixed powder distribution there was close to homogeneous by observing the simulated powder fluid structure at the moment of 0.1 second (Figure 4). Argon gas flow carried pre-mixed powder to move following the powder feeder pipe with the interaction of argon gas flow-particle, then exited though the outlet of the pipe. A section of powder feeder pipe was selected to observe the powder distribution at the moment of 2.0 second in Figure 4. It can be clearly found that some blue particles were ahead of red particles. Since both kinds of particles were supplied at the inlet simultaneously, the powder distribution in Figure 4

indicates that blue particles (4047 Al) moved faster than the red particles (Cu). Pre-mixed powder movement in powder feeder pipe shown greatly clear separation phenomenon. A reference zone was defined underneath the pipe outlet. The particle concentration in the reference zone was quantified and then compared with experiment results.

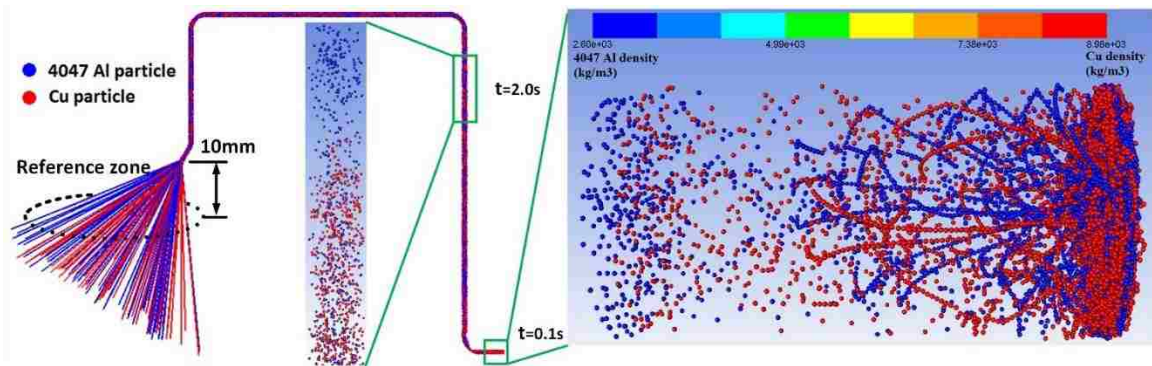


Figure 4. The powder distribution in simulation result

In order to clearly observe the pre-mixed powder separation in argon gas flow, ten different sections in powder feeder pipe were selected, which were depicted in Figure 5. The Figure 6 showed powder distributions in the ten pipe sections at the moment of 5 second. In the first section, both two powders were mixed and carried to move forward by argon gas flow. There was not clear separation phenomenon of pre-mixed powder in the first section. From the second section to the fourth section, there was not clear separation in powder flow. Beyond that, it is easy to find the powder distribution had less concentration than the first section. The separation phenomenon in pre-mixed powder flow was obviously observed in the section 5. Some 4047 Al particles were ahead of Cu particles, which indicates the 4047 Al particles had greater velocity than Cu particles. Since Al particles had smaller particle size and density, Al particles had greater acceleration compared with Cu particles by analyzing Eqn.9, in which particle acceleration is inversely

proportional with the product of particle density and particle diameter square. From the sixth section to the tenth section, all the particles were 4047 Al and there was not any Cu particles observed. 4047 Al particles moved faster than Cu particle so that a lot of Al particles ran ahead of Cu particles.

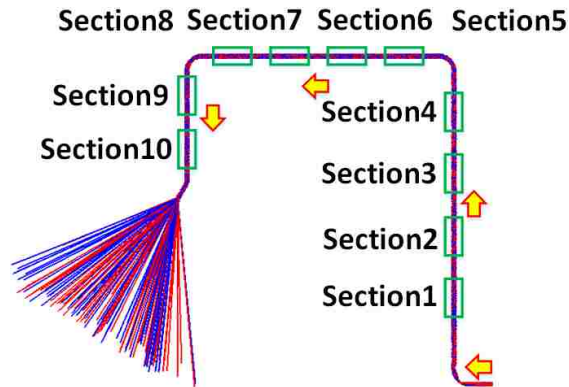


Figure 5. Ten sections in feeder pipe

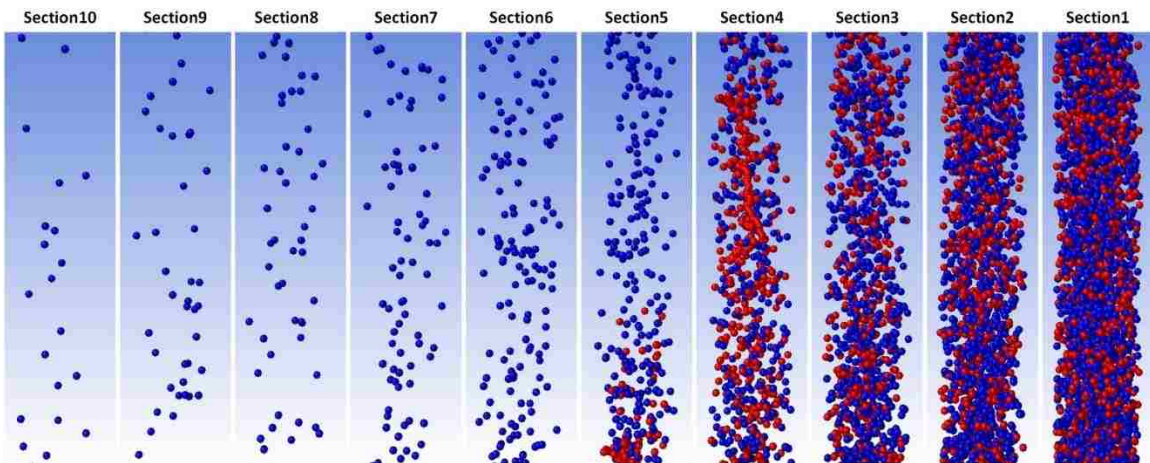


Figure 6. The simulated powder distribution in the ten pipe sections

The particle distribution in the section1 and section3 at five different moments were depicted in Figure 7 and Figure 8. The time interval between two adjacent moments was 0.05 second. The section1 located close to powder feeder inlet. By observing the particle

distributions in section1, it can be found that 4047 Al particles had tendency to surpass Cu particles as time went on. This tendency totally became powder separation in the section3. At the successive five moments, more and more 4047 Al particles surpassed and went ahead of Cu particles. This pre-mixed powder separation phenomenon will ruin the original composition ratio in powder mixture and finally resulted in composition deviation in deposit functional material.

The particle concentration in the reference zone was quantified and plotted in Figure 9. Blue color recorded the volume percentage of 4047 Al, while red color recorded the volume percentage of Cu. The time in the X-axis indicated the moments when the exiting particles from nozzle reached the reference zone. The time started when the first particle was blown to move at the inlet. In the beginning stage (approximately 0s ~ 4s), no particle sprayed out from the nozzle, so the volume percentage of two powders was zero. Starting from the moment of 4s, a flow of 4047 Al powder exited from the nozzle. After about 6 seconds, Cu particle start to spray out but the primary powder was 4047 Al. With time went by, more particles sprayed out from powder feeder nozzle, the primary particles are still 4047 Al, but whose volume percentage was decreasing gradually. In stark contrast, the volume percentage of Cu was gradually increasing. At the moment of 18.6 s, Cu and 4047 Al had approximately same volume percentage. Then from the moment of 18.6s to the end, Cu powder volume percentage surpassed the 4047 Al powder volume percentage, it was because more and more accumulated Cu particles behind Al particle sprayed out from the nozzle.

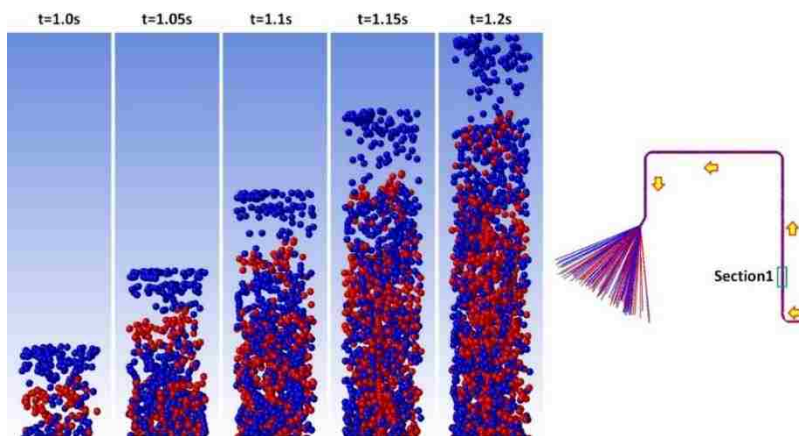


Figure 7. The powder distribution in section1 at different moments

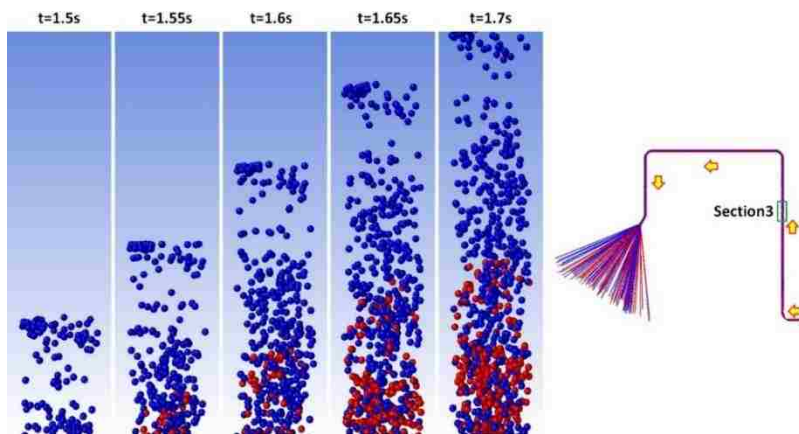


Figure 8. The powder distribution in section3 at different moments.

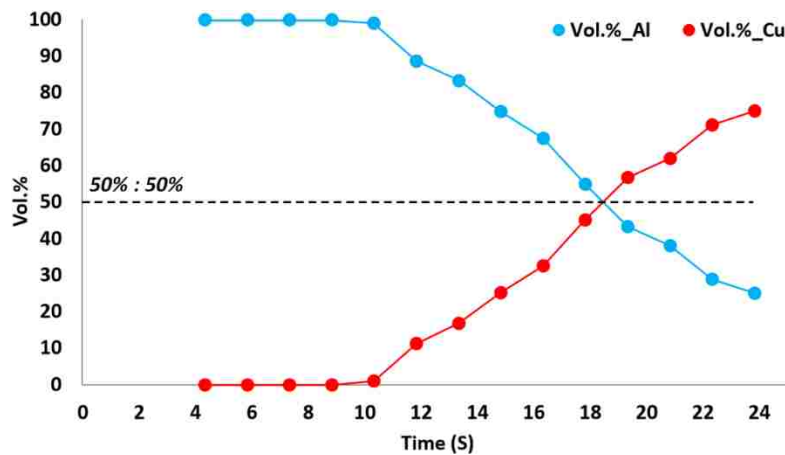


Figure 9. Powder quantification results

5. EXPERIMENTAL VALIDATION

In order to validate the simulated results, an experiment to analyze and quantify the pre-mixed powder distribution was operated by authors[1, 13]. The experiment set-up is schematically shown in Figure 10. A commercial powder feeder (Bay State Surface Technologies, Inc, Model-1200) was used to supply pre-mixed powder. Before experiment, the two metal powders were mixed for 30 mins with TURBULA Shaker-Mixer, which is a commercial equipment for the homogeneous mixing of powders with different specific weights and particle sizes. A piece of 6061 Aluminum alloy plate, paved with sticky epoxy resin, was fixed on two linear motors to move following the generated path. The idea of this experiment is to use the sticky epoxy resin layer to collect the pre-mixed 4047 Al and Cu powders spraying out from the nozzle. The optical microscopy was used to observe the powder pattern adhered on epoxy resin layer.

The operating parameters in the experiment were same with Table.1. After the epoxy resin solidified, powder pattern formed in the epoxy resin layer. 87 observed zones with the size of 4mm by 3mm distributed with uniform-interval along the central line of the powder path were selected for microscopic particle patterns observation. Then the distribution of different particles in the pattern was quantified. Due to the color difference of 4047 Al and Cu particles, the image processing software Image-J was used to mark these two kinds of particles in each observed zone, then count the particle numbers of two powders. Since particle sizes were known, the volume percentage of two powders in each observed zone can be calculated by Eqn.22 and Eqn.23. The powder volume percent quantification idea in the experiment was schematically illustrated in Figure 10.

$$Vol_{powder} = N_{particle} \times \frac{4}{3} \pi r_{mean}^3 \quad (22)$$

$$Vol. \%_{powder1} = 100 \times \frac{Vol_{powder1}}{Vol_{powder1} + Vol_{powder2}} \quad (23)$$

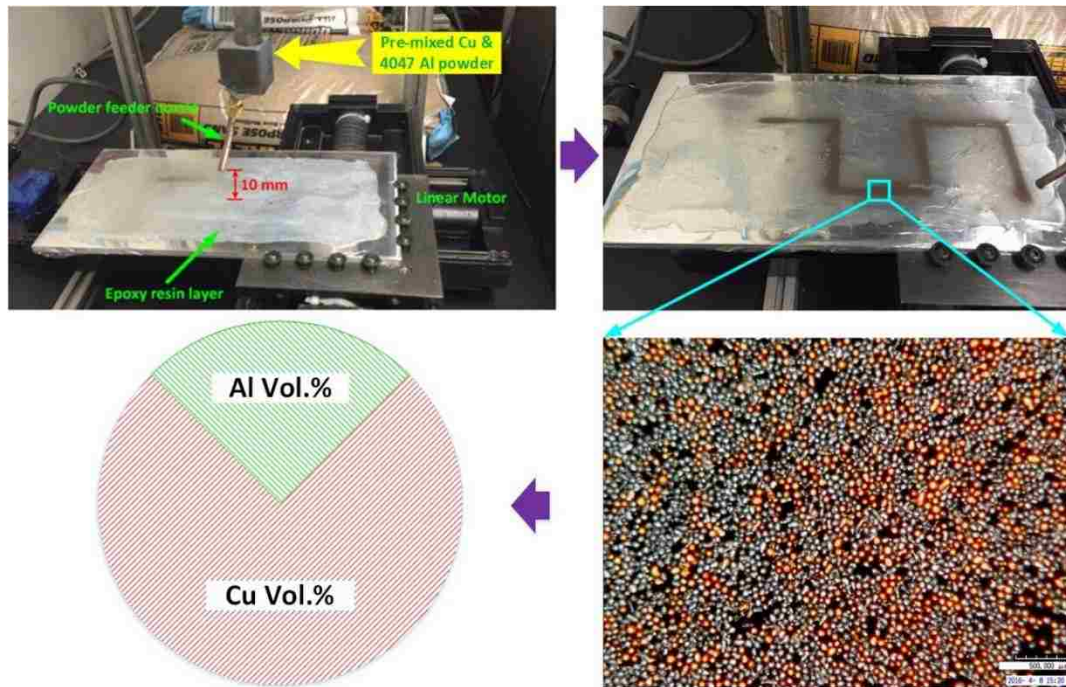


Figure 10. Experiment set-up and powder volume percent quantification.

The experimental validation result was shown in Figure 11. Dot plots recorded the simulated volume percentages of two powders, while diamond plots recorded the volume percentages of both powders in the experiment. Different colors indicated different kinds of powder. For the simulation results, the time in the X-axis indicated the moments when the exiting particles from nozzle reached the reference zone. Then for the experiment results, the time in the X-axis was used to indicate the moments when the particles in the corresponding observation zone reached the epoxy resin.

In Figure 11, the powder separation was obviously observed in both simulation and experiment results. In the beginning stage (approximately 0s ~ 4s), neither of Cu and 4047 Al sprayed out from the nozzle, so the volume percentages of two powders were zero. This vacant period was predicted by modeling and validated by the experiment. Starting from the moment of 4s, a flow of pre-mixed powder exited from the nozzle, in which 4047 Al was the primary particles. With time increasing, more particles sprayed out from powder feeder nozzle, the primary particles were still 4047 Al, but whose volume percentage was decreasing gradually. In stark contrast, the volume percentage of Cu was gradually increasing. At the moment of 21s in the experiment, Cu and 4047 Al had approximately same volume percentage. Then from the moment of 21s to the end, Cu powder volume percentage surpassed the 4047 Al powder volume percentage, it was because more and more accumulated Cu particles behind Al particle sprayed out from the nozzle. The intersecting moment in modeling was close to 18.6 s, which was 2 s earlier compared to experiment. Since both powders started to transit simultaneously from powder feeder pipe inlet, and 4047 Al particle had bigger acceleration than Cu particle according to the Eqn. 1, 4047 Al moved faster and exited from nozzle earlier than Cu particle. The powder volume percentage history in Figure 12 implied the pre-mixed powder separation since the two powders' volume percentage were not uniform and kept changing, although they were designed as 50%:50%. The modeling results had same tendency in volume percentage with experiment results. Modeling result had greater volume percentage of 4047 Al and less Cu particle volume percentage before the intersecting moment, but less 4047 Al particle and more Cu particle after the moment. As a whole, the modeling results, such as volume

percentages of two powders, the powder separation phenomenon, can match the experimental results well.

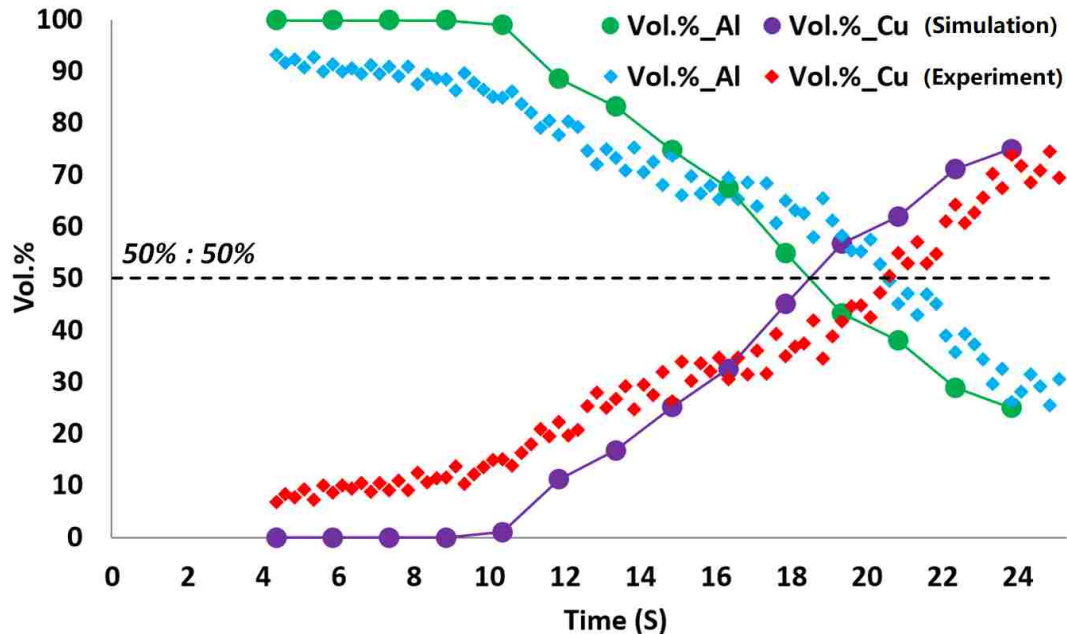


Figure 11. Experimentally validating the simulation result.

6. CONCLUSION

This study investigated the flow behaviors of pre-mixed powder supplied for LMD, and presented a comprehensive CFD-DEM model, which analyzed the powder separation in pre-mixed powder flow. Some conclusions were summarized as follows.

By solving discrete particle acceleration equations coupled with continuity equations and momentum equations for argon gas, the dynamic behavior of pre-mixed flow was simulated. The modeling results show that 4047 Al particle came out first from the nozzle comparing with the Cu particle. This is because 4047 Al particle's greater acceleration drove it to move faster than Cu particle. 4047 Al powder's volume percentage was greater than Cu powder, then experienced gradual decrease coupled with increasing

Cu powder volume percentage. As time went on, more and more accumulated Cu particles behind Al particle sprayed out from the nozzle, so that Cu powder volume percentage became greater than Al powder gradually. An intersecting moment ($t=18.6s$) happened when Al powder and Cu powder shifted their volume percentages. The modeled powder volume percentages were validated by the experiment result, but the intersecting moment in modeling was 2 s earlier compared to intersecting moment in the experiment. The reported CFD-DEM model was proved to be a powerful tool to investigate the pre-mixed powder's dynamic fluid behavior in LMD process. The study results, including volume percentages of two powders and the powder separation phenomenon, provided valuable reference for further analysis in fabricating functional material using LMD.

REFERENCES

- [1] Li, W., Zhang, J., Zhang, X., and Liou, F., 2017, "Effect of optimizing particle size on directed energy deposition of Functionally Graded Material with blown Pre-Mixed Multi-Powder," *Manufacturing Letters*, 13, pp. 39-43.
- [2] Carroll, B. E., Otis, R. A., Borgonia, J. P., Suh, J.-o., Dillon, R. P., Shapiro, A. A., Hofmann, D. C., Liu, Z.-K., and Beese, A. M., 2016, "Functionally graded material of 304L stainless steel and inconel 625 fabricated by directed energy deposition: Characterization and thermodynamic modeling," *Acta Materialia*, 108, pp. 46-54.
- [3] Schwendner, K. I., Banerjee, R., Collins, P. C., Brice, C. A., and Fraser, H. L., 2001, "Direct laser deposition of alloys from elemental powder blends," *Scripta Materialia*, 45(10), pp. 1123-1129.
- [4] Li, W., Yan, L., Karnati, S., Liou, F., Newkirk, J., Taminger, K. M. B., and Seufzer, W. J., 2017, "Ti-Fe intermetallics analysis and control in joining titanium alloy and stainless steel by Laser Metal Deposition," *Journal of Materials Processing Technology*, 242, pp. 39-48.
- [5] Li, W., Liou, F., Newkirk, J., Taminger, K. M. B., and Seufzer, W. J., 2017, "Investigation on Ti6Al4V-V-Cr-Fe-SS316 Multi-layers Metallic Structure Fabricated by Laser 3D Printing," *Scientific Reports*, 7(1), p. 7977.

- [6] Li, W., Liou, F., Newkirk, J., Taminger, K. M. B., and Seufzer, W. J., 2017, "Ti6Al4V/SS316 multi-metallic structure fabricated by laser 3D printing and thermodynamic modeling prediction," *The International Journal of Advanced Manufacturing Technology*, pp. 1-13.
- [7] Li, W., Karnati, S., Kriewall, C., Liou, F., Newkirk, J., Taminger, K. M. B., and Seufzer, W. J., 2017, "Fabrication and Characterization of a Functionally Graded Material from Ti-6Al-4 V to SS316 by Laser Metal Deposition," *Additive Manufacturing*.
- [8] Li, W., Yan, L., Chen, X., Zhang, J., Zhang, X., and Liou, F., 2018, "Directed energy depositing a new Fe-Cr-Ni alloy with gradually changing composition with elemental powder mixes and particle size'effect in fabrication process," *Journal of Materials Processing Technology*, 255, pp. 96-104.
- [9] Li, W., Chen, X., Yan, L., Zhang, J., Zhang, X., and Liou, F., 2017, "Additive manufacturing of a new Fe-Cr-Ni alloy with gradually changing compositions with elemental powder mixes and thermodynamic calculation," *The International Journal of Advanced Manufacturing Technology*.
- [10] Chen, X., Yan, L., Li, W., Liou, F., and Newkirk, J., 2016, "Effect of powder particle size on the fabrication of ti-6al-4v using direct laser metal deposition from elemental powder mixture," vol, 6, pp. 348-355.
- [11] Yan, L., Yan, L., Chen, X., Chen, X., Li, W., Li, W., Newkirk, J., Newkirk, J., Liou, F., and Liou, F., 2016, "Direct laser deposition of Ti-6Al-4V from elemental powder blends," *Rapid Prototyping Journal*, 22(5), pp. 810-816.
- [12] Yan, L., Li, W., Chen, X., Zhang, Y., Newkirk, J., Liou, F., and Dietrich, D., 2016, "Simulation of Cooling Rate Effects on Ti-48Al-2Cr-2Nb Crack Formation in Direct Laser Deposition," *JOM*, pp. 1-6.
- [13] Li, W., Karnati, S., Zhang, Y., and Liou, F., 2017, "Investigating and Eliminating Powder Separation in Pre-mixed Powder Supply for Laser Metal Deposition Process," *Journal of Materials Processing Technology*.
- [14] Pan, H., Sparks, T., Thakar, Y. D., and Liou, F., 2006, "The investigation of gravity-driven metal powder flow in coaxial nozzle for laser-aided direct metal deposition process," *Journal of manufacturing science and engineering*, 128(2), pp. 541-553.
- [15] Pan, H., and Liou, F., 2005, "Numerical simulation of metallic powder flow in a coaxial nozzle for the laser aided deposition process," *Journal of Materials Processing Technology*, 168(2), pp. 230-244.

- [16] Tan, H., Zhang, F., Wen, R., Chen, J., and Huang, W., 2012, "Experiment study of powder flow feed behavior of laser solid forming," *Optics and Lasers in Engineering*, 50(3), pp. 391-398.
- [17] Pinkerton, A. J., and Li, L., 2002, "A verified model of the behaviour of the axial powder stream concentration from a coaxial laser cladding nozzle," *Proceedings of ICALEO*.
- [18] Wen, S., Shin, Y., Murthy, J., and Sojka, P., 2009, "Modeling of coaxial powder flow for the laser direct deposition process," *International Journal of Heat and Mass Transfer*, 52(25), pp. 5867-5877.
- [19] Lia, W., Zhanga, J., Karnatia, S., Zhanga, Y., Lioua, F., Newkirkb, J., Taminger, K., and Seufzerc, W., "MODELING AND EXPERIMENTAL INVESTIGATION OF PRE-MIXED MULTI-POWDER FLOW IN FABRICATING FUNCTIONAL GRADIENT MATERIAL BY LASER METAL DEPOSITION PROCESS."
- [20] Guide, A. F. U., 2011, "Release 14.0, ANSYS Fluent User Manual," Inc., November.
- [21] Morsi, S., and Alexander, A., 1972, "An investigation of particle trajectories in two-phase flow systems," *Journal of Fluid mechanics*, 55(02), pp. 193-208.
- [22] Serag-Eldin, M., and Spalding, D., 1979, "Computations of three-dimensional gas-turbine combustion chamber flows," *Journal of Engineering for Power*, 101(3), pp. 326-336.
- [23] Launder, B. E., and Spalding, D. B., 1972, "Lectures in mathematical models of turbulence."
- [24] Deen, N., Annaland, M. V. S., Van der Hoef, M., and Kuipers, J., 2007, "Review of discrete particle modeling of fluidized beds," *Chemical Engineering Science*, 62(1), pp. 28-44

III. MODELING ANALYSIS OF ARGON GAS FLOW RATE'S EFFECT ON PRE-MIXED POWDER SEPARATION IN LASER METAL DEPOSITION AND EXPERIMENTAL VALIDATION

Wei Li, Xinchang Zhang, and Frank Liou

Department of Mechanical and Aerospace Engineering

Missouri University of Science and Technology, Rolla, Missouri 65409, U.S.A.

ABSTRACT

Pre-mixed powder is frequently-used powder supply to fabricate functional gradient material by Laser Metal Deposition (LMD). Argon gas flow blows the powder mixture following feeding pipe to melt pool in the LMD process. The powder mixture easily separates since the ingredient particles have different accelerations which are caused by different densities and sizes under the dynamic interaction with argon gas flow. This study investigated the argon gas flow rate's effect on pre-mixed powder separation using modeling methodology. Three argon gas flow rates: 6 m/s, 7 m/s, and 8 m/s were selected, analyzed, and compared based on their effects on powder mixture separations. Pre-mixed Cu and 4047 Al powders with equal volume percentages (50% to 50%) were investigated during their transportation process under three argon gas flow rates. The volume percentage of each kind of powder was plotted by quantifying the distribution of different particles after exiting the nozzle. It can be found that the intersection point of both powder volume percentages appeared increasingly earlier along with the increasing argon gas flow rate. The results from this study are valuable contributions to the research of functional graded materials fabrication with pre-mixed powder through LMD process.

1. INTRODUCTION

As a successful additive manufacturing process, Laser Metal Deposition (LMD) has gained great popularity to fabricate functional materials which can be specialized to satisfy various property or functionality requirements as the usage and working conditions demands. During the part's fabricating process, the needed functional composition can be obtained by melting pre-mixed powders, which have defined composition ratios to fulfill the utilization requirement [1, 2]. Most researchers utilized LMD process to manufacture the functional materials with customized designs, and have completed lots of material characterization and involved studies. Li [3] used laser metal deposition process to deposit a new Fe-Cr-Ni alloy with gradually changing compositions. Fe, Cr, Ni elemental powders were pre-mixed with gradually increasing Ni content in order to acquire the phase gradient distribution from ferrite to austenite. Li and Liou [4] demonstrated similar feasibility by fabricating a novel customized structure which successfully joined stainless steel and titanium alloy by means of LMD process with elemental powder feedstocks. Carroll and Otis [5] fabricated a customized material with functionally graded composition change from SS 304L to Inconel 625 by LMD process with pre-mixed powder as the feedstock. Designed variation in material properties throughout part's volume can be achieved from gradual changes in the composition to meet up with the design requirements.

The procedure of fabricating functional material by LMD was schematically depicted in Figure 1. Corresponding to the composition requirements, several kinds of alloy or metal elemental powders are weighed. The weight percentages (wt.%) or volume percentages (vol.%) should meet the demanded chemical composition ratio in the

functional materials. After that, all the weighed powders are mixed up adequately using suitable blending equipment. This blended powder is then applied as the powder supply for LMD process. An important advantage of pre-mixed powder is flexibility. The powder feedstocks can be produced with any chemical composition ratio. In addition, the composition of powder is able to be modified flexibly. More than that, because pre-mixed powder is from mixing some basic alloy or elemental powder, manufacturing cost is effectively saved.

During the LMD process, metal powder is driven and carried by argon gas flow through the powder feeder pipe and nozzle[6, 7]. The particle's movement is caused by the argon gas fluid medium's flow motion and fluctuation[8, 9]. Since the particles in the powder mixture have different densities and sizes, under the same argon gas flow, the movement of powders will not be uniform in powder feeder pipe. Lighter and smaller particles could move faster while heavier and bigger particles could lag behind. This kind of pre-mixed powder separation may cause the deviation from the original composition ratio. In functional material, the material composition ratio in any different area is required strictly. The pre-mixed powder separation will alter the composition ratio, and default the material performance. The argon gas flow is the main driving force to separate the pre-mixed powder. Therefore, it is greatly necessary to investigate the argon gas flow rate's effect on pre-mixed powder separation.

Powder feeding process in LMD is a standard fluid-particle system, which is composed of argon gas flow and metal powder. An effective modeling methodology to analyze the above fluid-particle system is a coupled Computational Fluid Dynamics method and Discrete Element Method (CFD-DEM)[10], which has sufficient consideration

of particle-particle collisions and fluid-particle interactions. The DEM is Lagrangian method, in which all particles in the computational domain are tracked by explicitly to calculate the particle trajectories[11, 12]. The DEM method is capable of solving the contact forces that generated by the particles collision, which is modelled by the Spring collision law[13-15]. The CFD method is employed to simulate the gas fluid-particle interaction, particle's dynamic behavior in argon gas flow, especially deeply understand the pre-mixed powder dynamic behavior[16]. A CFD model mainly includes three types of equations: continuity equation of mass; momentum conservation equations, and k- ϵ kinetic energy equations[17].

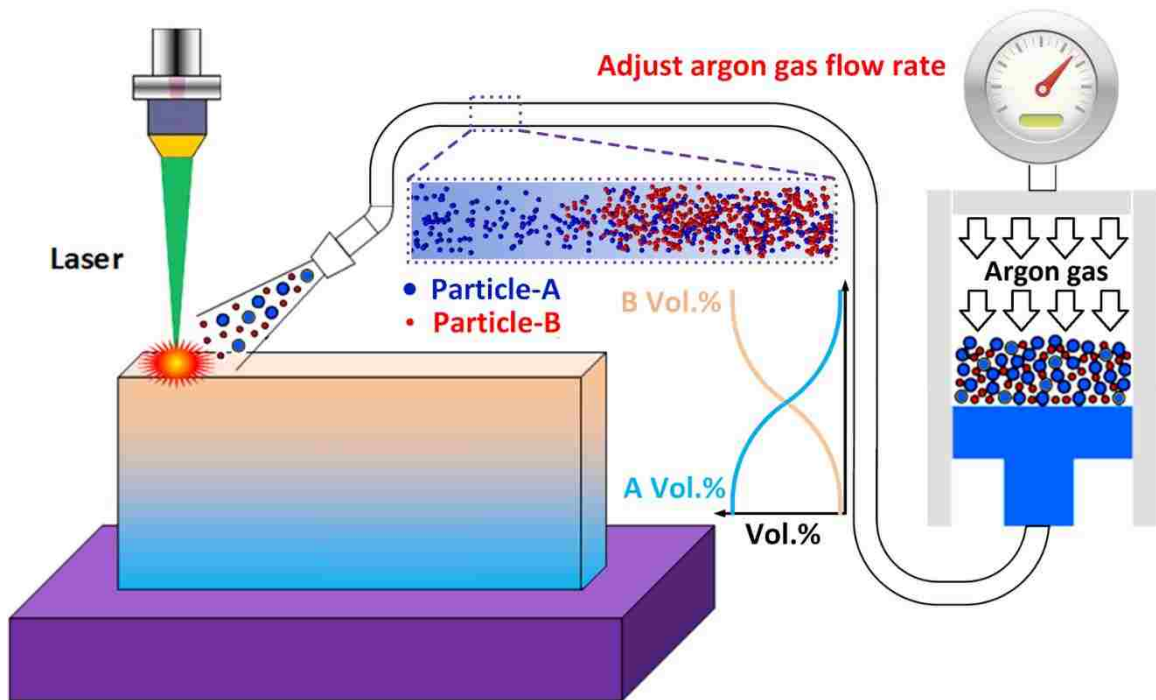


Figure 1. Schematic illustration of fabricating customized material by LMD

This study employed a comprehensive CFD-DEM model to analyze the argon gas flow rate's effect on powder separation in pre-mixed powder supplied for LMD process.

Three argon gas flow rates: 6 m/s, 7 m/s, and 8 m/s were selected and compared. Pre-mixed Cu and 4047 Al powders with equal volume percentages (50% to 50%) were investigated during their transportation process under the three argon gas flow rates. All particles' dynamic flow behaviors and the powder distributions were simulated, observed, and quantified. To prove the correctness of the simulation results, an experiment done by author before was reviewed.

2. MODELING PROCEDURE

2.1. CALCULATION DOMAIN

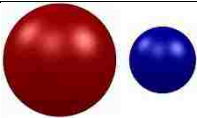
CFD-DEM model was used to simulate the powder flow in powder feeder pipe, which was designed with a 3-dimensional calculation domain. The powder feeder pipe shape was designed like this to make the calculation domain close to the real experiment condition [19]. The boundary condition of inlet was set as velocity inlet boundary, which was indicated with blue color. The velocities of argon gas flow and pre-mixed powder flow were applied at this boundary condition. Powder feeder pipe wall, which was indicated with magenta, was set as wall boundary condition. In computational fluid mechanics, wall means there is not any mass, flow, pressure passing through the wall. A calculation domain for powder spraying behavior was defined near the outlet nozzle of powder feeder pipe, whose boundary was indicated with black color. Outflow boundary condition was used surrounding the powder spraying domain. The outflow boundary is used to simulate the boundary condition where unknown outlet velocity and pressure happen but follow the developing process of fluid flow and conservation requirement. The direction of nozzle was leaning at 30 degree angle with the vertical pipe.

2.2. POWDER DESCRIPTION AND OPERATING PARAMETERS

To validate the modeling, two types of powders were used in the experiment authors did before. Pure Cu powder and 4047 Al powder were supplied from Atlantic Equipment Engineers. There were two reasons behind choosing these two powders. Firstly, Cu particles are red or close to red, while 4047 Al is of gray color. The color difference makes it easy to differentiate between these two particles in the experiments. Secondly, the density of Cu particle is 8.94 g/cm³, while 4047 Al's density is only 2.6 g/cm³. The density of Cu is approximately three times that of 4047 Al density. According to particle acceleration equation, particle acceleration is inversely proportional to particle density. Significant difference in density is expected to cause significant difference in particle acceleration. Therefore, the separation of pre-mixed powder is expected to be easy to observe. Figure 4 depicts the two kinds of powder particles through optical microscope images. Both types of particles were observed to be spherical or close to be spherical in shape. After sieve analysis of both powder, the Cu powder with the particle size distribution of 75-106 μm , and the 4047 Al powder with the particle size distribution of 45-75 μm , were selected.

The operating parameters in the modeling calculation were shown in Table.1, which were same as the experiment [1] done before. 4047 Al powder with the particle diameter range (45-75 μm), and Cu powder with the particle diameter range (75-106 μm) were mixed in the volume percentage ratio of 50%:50%. In author's lab, the argon gas flow rate was set as 6 m/s, which has been tested and verified to have satisfied deposition quality. Therefore, the argon gas flow rates were selected as 6 m/s, 7 m/s, and 8 m/s, to compare the argon gas flow rate's effect on powder mixture separation.

Table.1. The operating parameters in the modeling

Parameter	Value		
Schematic particles (Blue-Al; Red-Cu)			
4047 Al particle diameter	45-75 μm		
Cu particle diameter	75-106 μm		
Vol.% ratio	50%:50%		
Argon gas flow rate	6 m/s	7m/s	8m/s

3. SIMULATION RESULTS AND DISCUSSION

Pre-mixed powder distribution simulated by the CFD-DEM modeling was depicted in Figure 2. Blue color and red color were used to indicate the trajectories of 4047 Al particle and Cu particle respectively. A reference zone was defined underneath the pipe outlet. The particle concentration in the reference zone was quantified and then compared with experiment results. In order to clearly observe the pre-mixed powder distribution in argon gas flow, ten different sections in powder feeder pipe were selected, which were depicted in Figure 2. The powder distributions in the ten pipe sections shown in Figure 3 were at the moment of 5 second under three argon gas flow rates, 6m/s, 7m/s, and 8m/s. Think of the simulated powder distribution with 6m/s argon gas flow rate first. In the first section, both two powders were mixed and moved forward carried by argon gas flow. There was not clear separation phenomenon of pre-mixed powder in the first section. From the second section to the fourth section, there was not clear separation in powder flow. Beyond that, it is easy to find the powder distribution had less concentration than the first section. The separation phenomenon in pre-mixed powder flow was obviously observed in the

section 5. Some 4047 Al particles were ahead of Cu particles, which indicates the 4047 Al particles had greater velocity than Cu particles. Since Al particles had smaller particle size and density, Al particles had greater acceleration compared with Cu particles by referring to particle acceleration equation, in which particle acceleration is inversely proportional with the product of particle density and particle diameter square. From the sixth section to the tenth section, all the particles were 4047 Al and there was not any Cu particles observed. 4047 Al particles moved faster than Cu particle so that a lot of Al particles ran ahead of Cu particles.

The powder distributions under argon gas flow rates of 7 m/s and 8 m/s were depicted in Figure 3b and Figure 3c. It is easy to observe that the powder separation under the bigger argon gas flow rate was in advance of the powder separation under the smaller argon gas flow rate. Compare to the case of 6 m/s, the powder separation happened in section 7 under 7 m/s argon gas flow rate; and the powder separation took place in section 8 under 8 m/s argon gas flow rate. Bigger argon gas flow rate caused relatively bigger drag force to particles, so that powder separation can be much faster and more obvious.

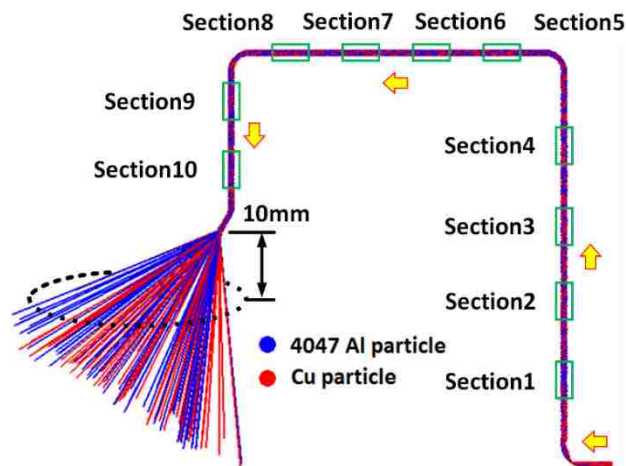
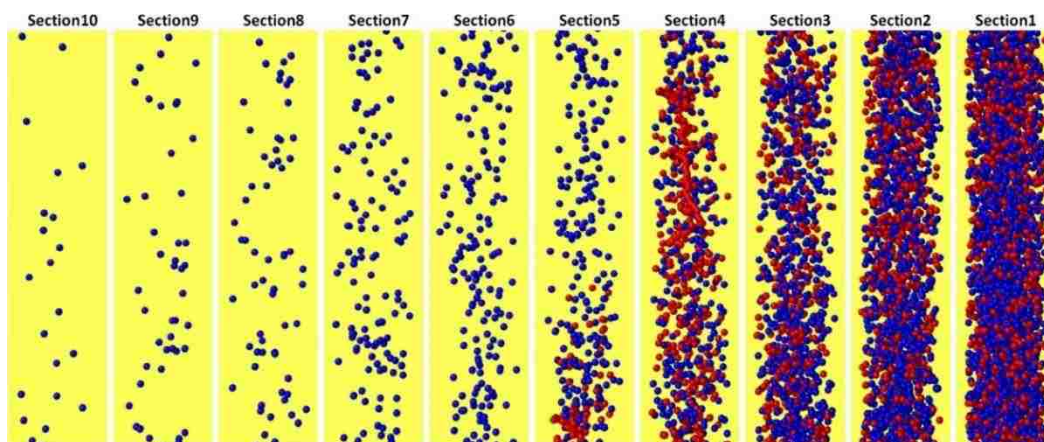
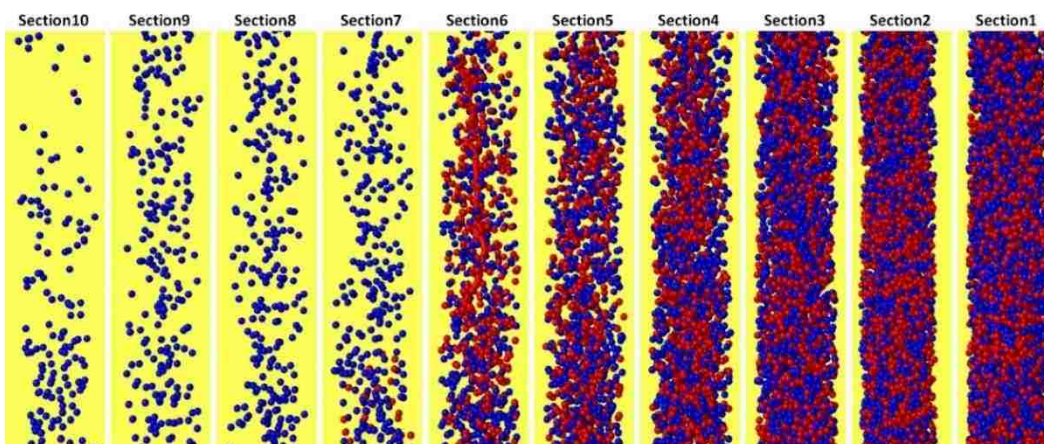


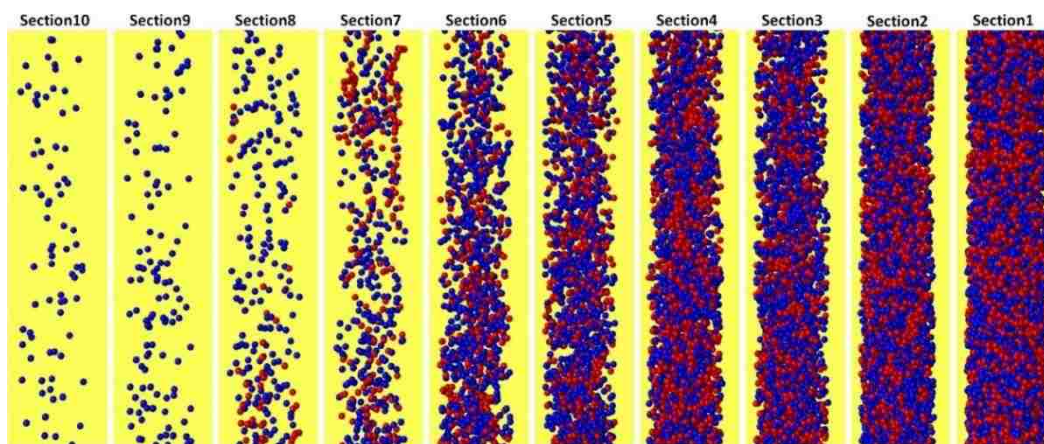
Figure 2. Ten sections in feeder pipe.



(a). Argon gas flow rate: 6m/s



(b). Argon gas flow rate: 7m/s



(c). Argon gas flow rate: 8m/s

Figure 3. Simulated powder distribution in the ten pipe sections at the moment of 5s.

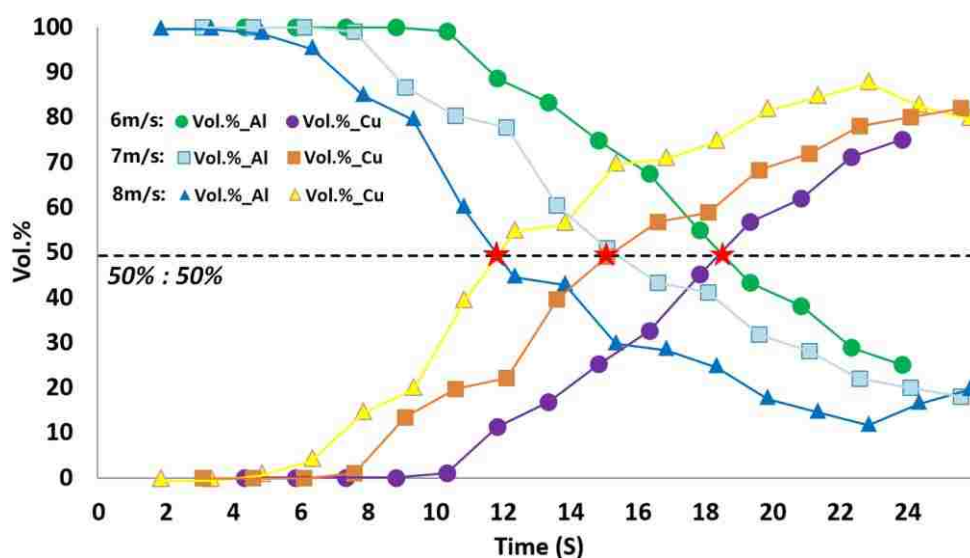


Figure 4. Powder quantification results.

The particle concentrations in the reference zone were quantified and plotted in Figure 4. The time in the X-axis indicated the moments when the exiting particles from nozzle reached the reference zone. The time started when the first particle was blown to move at the inlet. From the particle concentration plots for three argon gas flow rates, it can be clearly observed that 4047 Al powder exited from the nozzle earlier than Cu powder. Because Al particle has smaller particle size and lighter density than Cu particle, the acceleration of Al particle was greater than Cu particle, so that Al particle moved faster than Cu particle. With time went by, more particles sprayed out from powder feeder nozzle, the primary particles were still 4047 Al, but whose volume percentage was decreasing gradually. On the other hand, the Cu powder's volume percentage was gradually increasing over time. There was an intersection point of Al and Cu volume percentages. The reason was more and more accumulated Cu particles behind Al particle sprayed out from the nozzle. Therefore, Cu powder volume percentage surpassed the 4047 Al powder volume percentage. Another noteworthy result is the intersection point with higher argon gas flow

rate appeared earlier than the intersection point with lower argon gas flow rate. It was because higher argon gas flow rate caused bigger drag force to particles. As a result, powder separation occurred much faster than lower argon gas flow rate. This can also be found in the simulated powder distribution in Figure 3.

4. EXPERIMENTAL VALIDATION

With the purpose of validating correctness of the CFD-DEM model, an experiment operated by authors was reviewed. This experiment analyzed and quantified the pre-mixed powder distribution under the argon gas flow rate of 6 m/s [1]. A commercial powder feeder (Bay State Surface Technologies, Inc, Model-1200) was used to supply pre-mixed powder. Before experiment, the two metal powders were mixed for 30 mins with TURBULA Shaker-Mixer, which is a commercial equipment for the homogeneous mixing of powders with different specific weights and particle sizes. A piece of 6061 Aluminum alloy plate, paved with sticky epoxy resin, was fixed on two linear motors to move following the generated path. The idea of this experiment is to use the sticky epoxy resin layer to collect the pre-mixed 4047 Al and Cu powders spraying out from the nozzle. The optical microscopy was used to observe the powder pattern adhered on epoxy resin layer.

The experimental validation result was shown in Figure 5. Different colors and mark shapes indicated different powder volume percentages. For the simulation results, the time in the X-axis indicated the moments when the exiting particles from nozzle reached the reference zone. Then for the experiment results, the time in the X-axis was used to indicate the moments when the particles in the corresponding observation zone reached the epoxy resin.

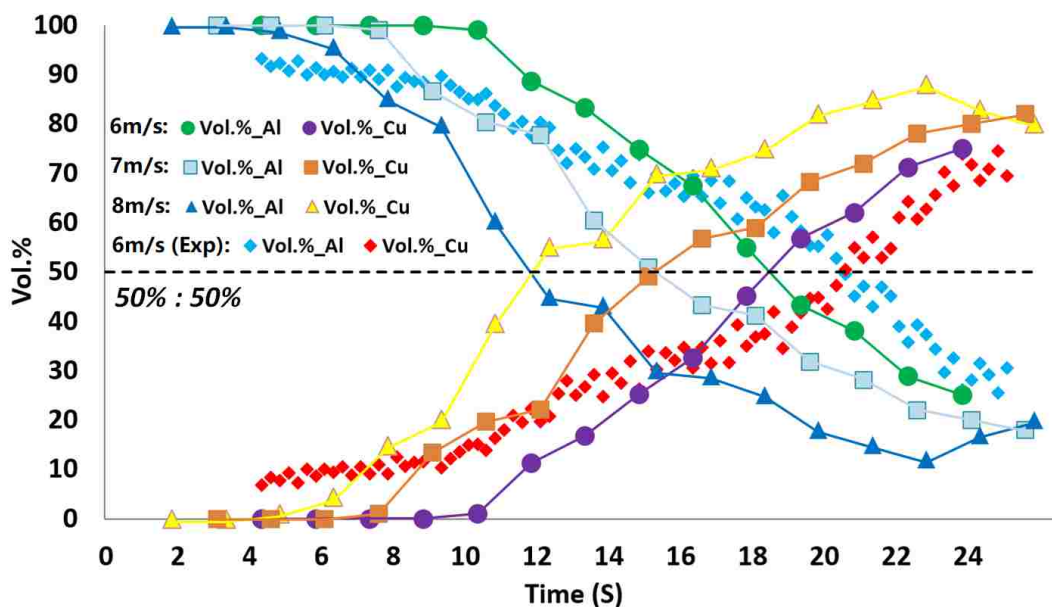


Figure 5. Experimental validating the model.

By observing the validation result under the 6 m/s argon gas flow rate, the powder separation was obviously found in both simulation and experiment results. In the beginning stage (approximately 0s ~ 4s), neither of Cu and 4047 Al sprayed out from the nozzle, so the volume percentages of two powders were zero. This vacant period was predicted by modeling and validated by the experiment. Starting from the moment of 4s, a flow of pre-mixed powder exited from the nozzle, in which 4047 Al was the primary particles. With time increasing, more particles sprayed out from powder feeder nozzle, the primary particles were still 4047 Al, but whose volume percentage was decreasing gradually. On the other hand, the volume percentage of Cu was gradually increasing. At the moment of 21s (intersection point) in the experiment, Cu and 4047 Al had approximately same volume percentage. Then from the moment of 21s to the end, Cu powder volume percentage surpassed the 4047 Al powder volume percentage, it was because more and more accumulated Cu particles behind Al particle sprayed out from the nozzle. The intersecting

moment in modeling was close to 18.6 s, which was 2 seconds earlier compared to experiment. Since both powders started to transit simultaneously from powder feeder pipe inlet, and 4047 Al particle had bigger acceleration than Cu particle according, 4047 Al moved faster and exited from nozzle earlier than Cu particle. The powder volume percentage history in Figure 5 implied the pre-mixed powder separation since the two powders' volume percentage were not uniform and kept changing, although they were designed as 50%:50%. The modeling results had same tendency in volume percentage with experiment results. Modeling result had greater volume percentage of 4047 Al and less Cu particle volume percentage before the intersecting moment, but less 4047 Al particle and more Cu particle after the moment. As a whole, the modeling volume percentages of two powders can match the experimental results well.

5. CONCLUSION

This paper applied a comprehensive CFD-DEM model to analyze argon gas flow rate's effect on pre-mixed powder separation in LMD process coupled with experimental validation. Some conclusions were summarized as follows.

By solving discrete particle acceleration equations coupled with continuity equations and momentum equations for argon gas, the dynamic behavior of pre-mixed flow was simulated. Since Al particle has smaller particle size and lighter density than Cu particle, the acceleration of Al particle was greater than Cu particle, so that Al particle moved faster than Cu particle. The separation phenomenon in pre-mixed powder was observed in both modeling result and experiment.

The pre-mixed powder separation generated the intersection point of Al and Cu powder volume percentage plots. Another noteworthy result is the intersection point with higher argon gas flow rate appeared earlier than the intersection point with lower argon gas flow rate. It was because higher argon gas flow rate caused bigger drag force to particles. As a result, powder separation occurred much faster than lower argon gas flow rate.

REFERENCES

- [1] Li, W., Zhang, J., Zhang, X., and Liou, F., 2017, "Effect of optimizing particle size on directed energy deposition of Functionally Graded Material with blown Pre-Mixed Multi-Powder," *Manufacturing Letters*, 13, pp. 39-43.
- [2] Li, W., Karnati, S., Zhang, Y., and Liou, F., 2018, "Investigating and eliminating powder separation in pre-mixed powder supply for laser metal deposition process," *Journal of Materials Processing Technology*, 254, pp. 294-301.
- [3] Li, W., Chen, X., Yan, L., Zhang, J., Zhang, X., and Liou, F., 2017, "Additive manufacturing of a new Fe-Cr-Ni alloy with gradually changing compositions with elemental powder mixes and thermodynamic calculation," *The International Journal of Advanced Manufacturing Technology*.
- [4] Li, W., Yan, L., Karnati, S., Liou, F., Newkirk, J., Taminger, K. M. B., and Seufzer, W. J., 2017, "Ti-Fe intermetallics analysis and control in joining titanium alloy and stainless steel by Laser Metal Deposition," *Journal of Materials Processing Technology*, 242, pp. 39-48.
- [5] Carroll, B. E., Otis, R. A., Borgonia, J. P., Suh, J.-o., Dillon, R. P., Shapiro, A. A., Hofmann, D. C., Liu, Z.-K., and Beese, A. M., 2016, "Functionally graded material of 304L stainless steel and inconel 625 fabricated by directed energy deposition: Characterization and thermodynamic modeling," *Acta Materialia*, 108, pp. 46-54.
- [6] Li, W., Liou, F., Newkirk, J., Taminger, K. M. B., and Seufzer, W. J., 2017, "Investigation on Ti6Al4V-V-Cr-Fe-SS316 Multi-layers Metallic Structure Fabricated by Laser 3D Printing," *Scientific Reports*, 7.
- [7] Li, W., Karnati, S., Kriewall, C., Liou, F., Newkirk, J., Taminger, K. M. B., and Seufzer, W. J., 2017, "Fabrication and Characterization of a Functionally Graded Material from Ti-6Al-4 V to SS316 by Laser Metal Deposition," *Additive Manufacturing*.

- [8] Zhu, H., Zhou, Z., Yang, R., and Yu, A., 2008, "Discrete particle simulation of particulate systems: a review of major applications and findings," *Chemical Engineering Science*, 63(23), pp. 5728-5770.
- [9] Li, W., Yan, L., Chen, X., Zhang, J., Zhang, X., and Liou, F., 2018, "Directed energy depositing a new Fe-Cr-Ni alloy with gradually changing composition with elemental powder mixes and particle size'effect in fabrication process," *Journal of Materials Processing Technology*, 255, pp. 96-104.
- [10] Zhao, J., and Shan, T., 2013, "Coupled CFD–DEM simulation of fluid–particle interaction in geomechanics," *Powder technology*, 239, pp. 248-258.
- [11] Parteli, E. J., and Pöschel, T., 2016, "Particle-based simulation of powder application in additive manufacturing," *Powder Technology*, 288, pp. 96-102.
- [12] Haeri, S., Wang, Y., Ghita, O., and Sun, J., 2017, "Discrete element simulation and experimental study of powder spreading process in additive manufacturing," *Powder Technology*, 306, pp. 45-54.
- [13] Guide, A. F. U., 2011, "Release 14.0, ANSYS Fluent User Manual," Inc., November.
- [14] Parteli, E. J., 2013, "Using LIGGGHTS for performing DEM simulations of particles of complex shapes with the multisphere method," In: *DEM6-6th International Conference on Discrete Element Methods and Related Techniques*, Golden USA.
- [15] Kloss, C., Goniva, C., Hager, A., Amberger, S., and Pirker, S., 2012, "Models, algorithms and validation for opensource DEM and CFD–DEM," *Progress in Computational Fluid Dynamics, an International Journal*, 12(2-3), pp. 140-152.
- [16] Zekovic, S., Dwivedi, R., and Kovacevic, R., 2007, "Numerical simulation and experimental investigation of gas–powder flow from radially symmetrical nozzles in laser-based direct metal deposition," *International Journal of Machine Tools and Manufacture*, 47(1), pp. 112-123.
- [17] Thompson, S. M., Bian, L., Shamsaei, N., and Yadollahi, A., 2015, "An overview of Direct Laser Deposition for additive manufacturing; Part I: Transport phenomena, modeling and diagnostics," *Additive Manufacturing*, 8, pp. 36-62.
- [18] Wen, S., Shin, Y., Murthy, J., and Sojka, P., 2009, "Modeling of coaxial powder flow for the laser direct deposition process," *International Journal of Heat and Mass Transfer*, 52(25), pp. 5867-5877.

- [19] Lia, W., Zhanga, J., Karnatia, S., Zhanga, Y., Lioua, F., Newkirkb, J., Tamingerc, K., and Seufzerc, W., "MODELING AND EXPERIMENTAL INVESTIGATION OF PRE-MIXED MULTI-POWDER FLOW IN FABRICATING FUNCTIONAL GRADIENT MATERIAL BY LASER METAL DEPOSITION PROCESS."
- [20] Morsi, S., and Alexander, A., 1972, "An investigation of particle trajectories in two-phase flow systems," *Journal of Fluid mechanics*, 55(02), pp. 193-208.
- [21] Pan, H., Sparks, T., Thakar, Y. D., and Liou, F., 2006, "The investigation of gravity-driven metal powder flow in coaxial nozzle for laser-aided direct metal deposition process," *Journal of manufacturing science and engineering*, 128(2), pp. 541-553.
- [22] Serag-Eldin, M., and Spalding, D., 1979, "Computations of three-dimensional gas-turbine combustion chamber flows," *Journal of Engineering for Power*, 101(3), pp. 326-336.
- [23] Launder, B. E., and Spalding, D. B., 1972, "Lectures in mathematical models of turbulence."
- [24] Deen, N., Annaland, M. V. S., Van der Hoef, M., and Kuipers, J., 2007, "Review of discrete particle modeling of fluidized beds," *Chemical Engineering Science*, 62(1), pp. 28-44.

**IV. CFD-DEM MODELING ANALYSIS OF PARTICLE SIZE
OPTIMIZATION'S EFFECT ON CONTROLLING PRE-MIXED POWDER
FLOW SEPARATION IN LASER METAL DEPOSITION**

Wei Li, Xinchang Zhang, Tan Pan, and Frank Liou

Department of Mechanical and Aerospace Engineering

Missouri University of Science and Technology, Rolla, Missouri 65409, U.S.A.

ABSTRACT

The separation in pre-mixed powder flow is a critical issue in fabricating Functional Gradient Material (FGM) using Laser Metal Deposition (LMD), since the powder mixture separation can ruin the original mixing composition ratio, which is designed to match the FGM. Authors invented a novel particle size optimization method as the solution to eliminate the powder separation and reduce the composition deviation. Through optimizing particle size, the acceleration of particles can be uniform or close to uniform, so that the original mixing composition can be maintained. In this research, the particle size optimization's effect on controlling pre-mixed powder separation was numerically analyzed with a comprehensive CFD-DEM model, which was based on the fundamentals of discrete element methodology and computational fluid dynamics. Through dealing with discrete particle force balance equations combined with argon gas's continuity equations and momentum equations, the powder mixture flow's dynamic behavior in feeder pipe and out of nozzle was simulated. The modeling results were validated by the experiment done by author before. It can be clearly observed that the powder separation was effectively controlled in both modeling and experimental results.

1. INTRODUCTION

Functional gradient material (FGM) is stimulating an increasing amount of research concentration, because it can be customized to fulfill numerous property or functionality requirements as the utilization and working conditions needs. Laser Metal Deposition (LMD) is a powerful manufacturing process to fabricate functional materials. Within the part's fabrication by LMD, the demanded functional composition can be gained by melting pre-mixed powders, which have specified composition ratios to satisfy the usage requirement [1]. Many researchers employed LMD process to manufacture the functional materials with customized designs, and have done a lot of material characterization and related analysis[2-6]. The pre-mixed powders included various powders and collocations.

The powder separation behavior was an important issue in manufacturing FGM through LMD. The separation in pre-mixed powder flow can cause composition deviation from the original composition ratio in fabricated functional material, which will default the material's function and value. Figure 1 is a schematic illustration depicting the feeding process of pre-mixed powders in LMD. Argon gas flow is applied to drive the powders following the powder feeder pipe, then going to the melt pool through the nozzle. Because the particles in the powder mixture have various densities and sizes, the movement of powders will not be uniform in powder feeder pipe under the same argon gas flow. Lighter and smaller particles could move faster while heavier and bigger particles could lag behind. The basic reason of powder separation is that the different types of particles have non-uniform moving velocities in powder feeder pipe. Due to the fact that powder mixture was supplied to the pipe inlet with constant initial velocity (zero velocity in general), the non-

uniform velocities are fundamentally caused by non-uniform accelerations. Based on the Lagrangian reference frame integrating the force balance on the particle in the gas fluid-particle interaction, the particle acceleration can be derived as follows [7].

$$a_p = \frac{18\mu}{\rho_p d_p^2} \frac{C_D Re}{24} (u - u_p) + \frac{g(\rho_p - \rho)}{\rho_p} \quad (1)$$

where a_p , u_p , ρ_p , and d_p are the acceleration, velocity, density, and diameter of particle, respectively. u and ρ are velocity and density of argon gas respectively. C_D is the drag coefficient which is dimensionless quantity. Re is Reynolds number and μ is the viscosity of argon gas flow. If only considering the particle property's effect, Eqn. (1) indicates that the particle acceleration is affected by the product of particle density and particle diameter square.

A standard LMD fluid-particle system is composed of argon gas flow and metal powder [8]. In this system, particle's movement is caused or driven by the argon gas fluid medium's flow motion and fluctuation [9]. An encouraging modeling methodology to analyze the above fluid-particle system is a coupled Computational Fluid Dynamics method and Discrete Element Method (CFD-DEM)[10], which has appropriate thought of particle-particle collisions and fluid-particle interactions. The DEM is Lagrangian method, in which all particles in the computational domain are tracked by explicitly to calculate the particle trajectories [11, 12]. The DEM method is capable of solving the contact forces that generated by the particles collision, which is modelled by the Spring collision law[13-15]. The CFD method is employed to simulate the gas fluid-particle interaction, particle's dynamic behavior in argon gas flow, especially deeply understand the pre-mixed powder dynamic behavior [16]. In a CFD model, three types of equations are mainly included:

continuity equation of mass; momentum conservation equations, and k- ϵ kinetic energy equations [17].

Based on the study of particle acceleration, this work introduced a novel particle size optimization method as the solution to eliminate the powder separation. The CFD-DEM modeling tool was used to simulate the particle fluid behaviors in powder feeder pipe, to demonstrate the effect of optimizing particle size in controlling pre-mixed powder separation. In addition, an experiment done by author was reviewed in this study. The modeling results was then validated by the experimental data.

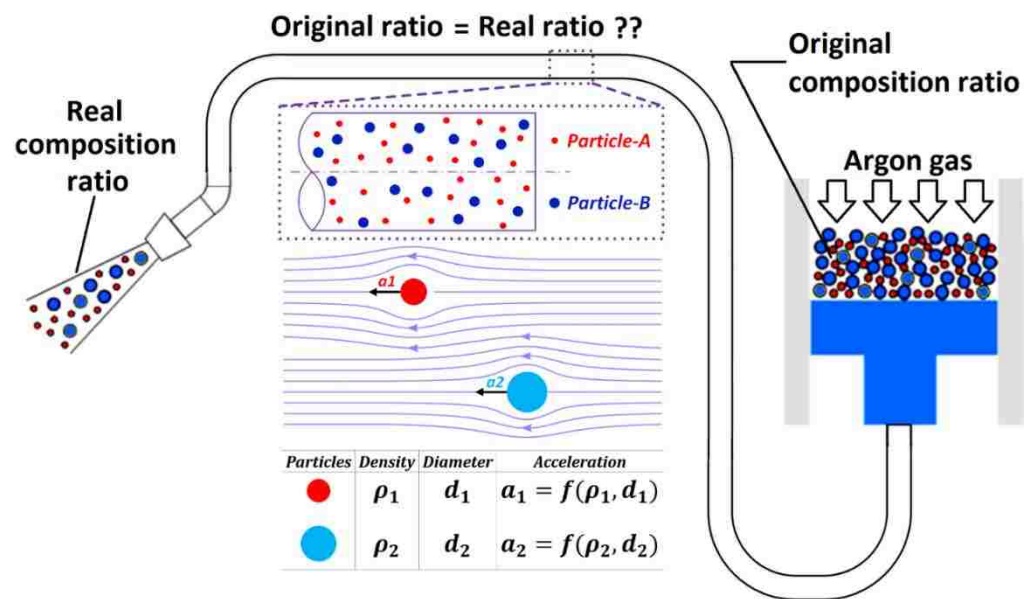


Figure 1. Schematic illustration of feeding process of pre-mixed powders.

2. EXPERIMENTAL REVIEW AND PARTICLE SIZE OPTIMIZATION APPROACH INTRODUCTION

Authors published a journal reference [18] which reported a novel particle size optimization idea through experimental approach. This particle size optimization idea

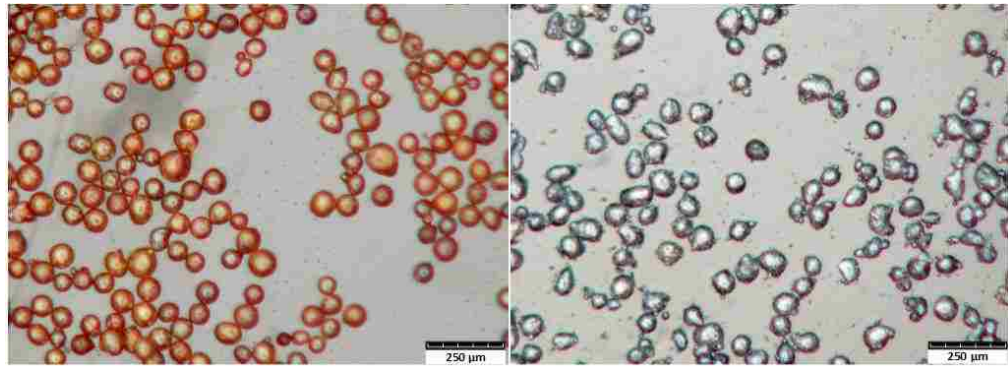
answered a question: how to address the powder mixture's separation in LMD processing functional material to reduce the composition deviation.

Two types of powders were used in the experiment. Pure Cu powder and 4047 Al powder were supplied from Atlantic Equipment Engineers. Figure 2 depicts the two types of powder particles through optical microscope images. The color difference of two powders gave convenience to distinguish them in the experiment. Both the Cu and 4047 Al particles were spherical or close to be spherical in shape. The particle size distributions of the two types of powder obtained by sieve analysis are listed in Table.1 and Table.2. The experiment set-up is schematically illustrated in Figure 3(a) and Figure 3(b). The pre-mixed powder was supplied by a commercial powder feeder (Bay State Surface Technologies, Inc, Model-1200). Before experiment, the two metal powders were mixed for 30 mins with TURBULA Shaker-Mixer, which is a commercial equipment for the homogeneous mixing of powders with different specific weights and particle sizes. Two linear motors controlled a piece of 6061 Aluminum alloy plate to move following a generated path. Sticky epoxy resin was paved on the plate in order to collect the pre-mixed 4047 Al and Cu powders spraying out from the nozzle. The powder pattern adhered on epoxy resin layer was observed with optical microscopy. 87 observed zones with the size of 4mm by 3mm distributed with uniform-interval along the central line of the powder path were selected for microscopic particle patterns observation. Then the distribution of different particles in the pattern was quantified. Due to the color difference of 4047 Al and Cu particles, the image processing software Image-J was used to mark these two kinds of particles in each observed zone, then count the particle numbers of two powders. Since particle sizes were known, the volume percentage of two powders in each observed zone

can be calculated by Eqn.2 and Eqn.3. The powder volume percent quantification idea in the experiment was schematically illustrated in Figure 3(c).

$$Vol_{powder} = N_{particle} \times \frac{4}{3} \pi r_{mean}^3 \quad (2)$$

$$Vol.\%_{powder1} = 100 \times \frac{Vol_{powder1}}{Vol_{powder1} + Vol_{powder2}} \quad (3)$$



(a)

(b)

Figure 2. Optical microscopic images for: (a) Cu particles; and (b) 4047 Al particles[18].

Table.1. Sieve analysis of pure Cu powder

Sieve type	+70 mesh	-70/+100 mesh	-100/+120 mesh	-120/+140 mesh	-140/+200 mesh	-200/+325 mesh
Size (μm)	>212	150-212	125-150	106-125	75-106	45-75
Percentage (%)	0.0	1.3	2.4	3.7	47.4	45.2

Table.2. Sieve analysis of 4047 Al powder

Sieve type	+70 mesh	-70/+100 mesh	-100/+120 mesh	-120/+140 mesh	-140/+200 mesh	-200/+325 mesh
Size (μm)	>212	150-212	125-150	106-125	75-106	45-75
Percentage (%)	1.1	2.8	5.4	20.3	42.5	27.9

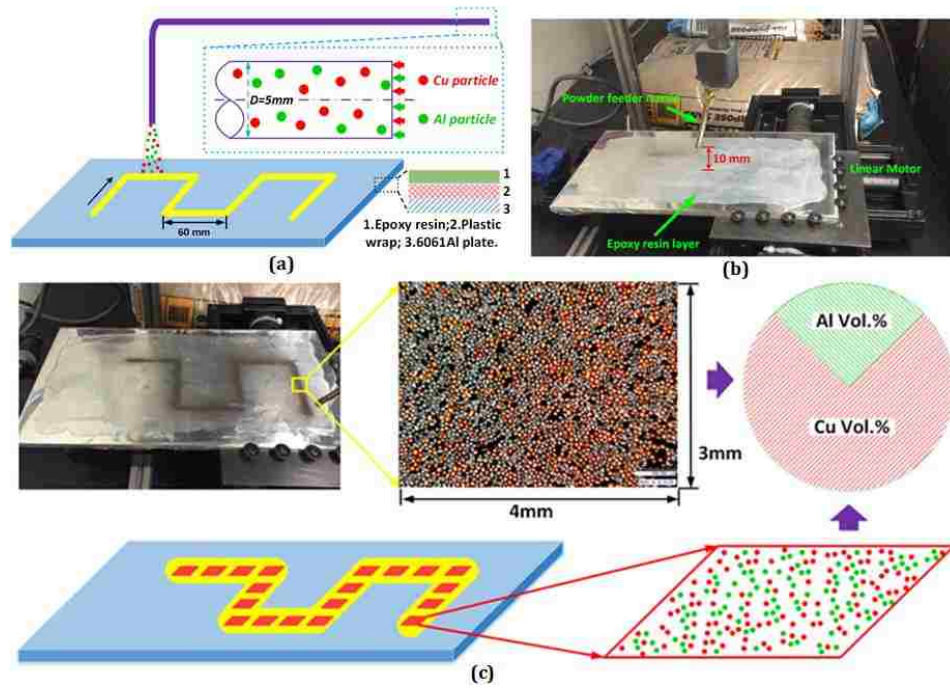


Figure 3. (a). Experiment design; (b). Experiment set-up; (c). Powder volume percent quantification[1].

The theory fundamental of the reported optimization idea is the particle acceleration equation which described the interaction of metal powder and argon gas flow in gas fluid-particle system. The particle acceleration (Eqn.1) is a classic first order differential equation with variable of particle velocity u_p . In the process of LMD, each particle has such a differential equation for itself to describe its dynamic movement in powder feeder pipe. The second term on the right side can be simplified as gravitational acceleration g because particle density ρ_p is much greater than argon gas density ρ . The first term on the right side contains several coefficients including argon gas flow velocity u , drag coefficient C_D , argon gas density ρ , and the product of particle diameter d_p and density ρ_p . The coefficients u , C_D , and ρ are same for all the particles, but the product of density and diameter square $\rho_p d_p^2$ varies for different types of powders. In this study, the two particle

densities ρ_{p_Cu} and ρ_{p_Al} , represent Cu particle density and 4047 Al particle density respectively. One ideal situation is, if Cu powder and 4047 Al powder have same density-diameter square products (in Eqn.4), then both type of particles will have uniform acceleration equations. The initial particle velocity is supposed as zero at powder feeder pipe orifice. Therefore, both types of particles will have almost same or very close velocity distribution and history, so that the separation of pre-mixed powder could be effectively eliminated.

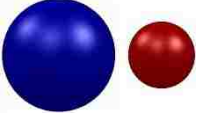
$$\rho_{p_Cu}d_{p_Cu}^2 = \rho_{p_Al}d_{p_Al}^2 \quad (4)$$

$$\frac{d_{p_Al}}{d_{p_Cu}} = \sqrt{\frac{\rho_{p_Cu}}{\rho_{p_Al}}} = \sqrt{\frac{8.94g/cm^3}{2.6g/cm^3}} = 1.854 \quad (5)$$

The Eqn.4 was rewritten in a new proportion format in Eqn.5, which explains an important criterion: if 4047 Al particle diameter is 1.854 times greater than Cu particle diameter, both type of particles will have same acceleration equations. Much closer the d_{p_Al}/d_{p_Cu} is to the ideal value, more effectively the powder mixture separation could be eliminated.

Based on the above analysis, one particle size optimization method was introduced. Sieve processing of Cu powder and 4047 Al powder separated these two powders into different size ranges (see in Table.1 and Table.2). Select the powders whose particle diameter ratio d_{p_Al}/d_{p_Cu} was equal or very close to the ideal value 1.854, then mix them together. Following the sieve processing result, 4047 Al powder with the particle diameter (75-106 μm), and Cu powder with the particle diameter range (45-75 μm) were selected and then mixed in the 50%:50% Vol.% ratio. The operating parameters in both experiment and modeling were shown in Table.3.

Table.3. The operating parameters in experiment and modeling

Schematic particles (Blue-Al; Red-Cu)	
4047 Al particle diameter	75-106 μm
Cu particle diameter	45-75 μm
d_{p_Al}/d_{p_Cu}	1.5
Vol.% ratio	50%:50%
Argon gas flow rate	6 m/s

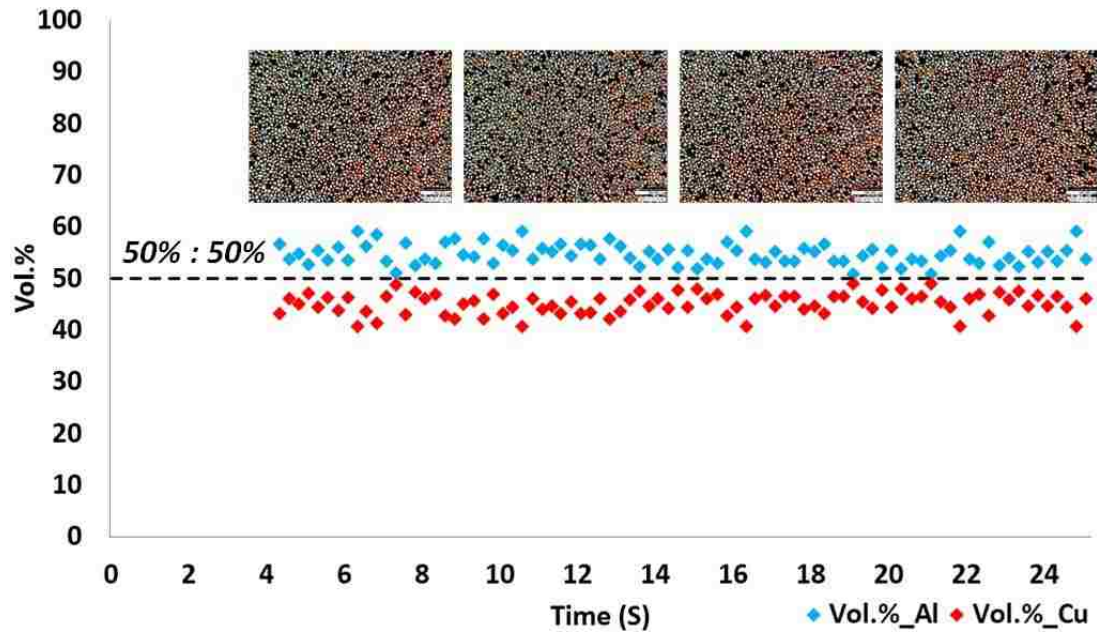


Figure 4. Quantification of pre-mixed powder composition patterns in experiment[18]

The quantification of pre-mixed powder composition patterns in experiment-2 was shown in Figure 4. Blue color recorded the volume percentage of 4047 Al, while red color recorded the volume percentage of Cu. The time in the X-axis indicated the moments when the particles in the relative observation zone reached the epoxy resin. By observing the optimized pre-mixed powder's composition distribution patterned in the epoxy resin

coating, the powder flow had basically constant volume percentages, which were close to 50%:50%. Four optical micrographs schematically illustrated the pre-mixed powder distribution at different observed zones in the particle pattern. There were not obvious differences of color distribution, which mean the powder composition ratio can keep approximately uniform. The quantification result and optical micrographs indicated that the pre-mixed powder separation can be effectively controlled by optimizing the particle size.

3. SIMULATION RESULTS AND DISCUSSION

Figure 5 depicted the pre-mixed powder distribution simulated by the CFD-DEM modeling. Blue color and red color were used to indicate the trajectories of 4047 Al particle and Cu particle respectively. Pre-mixed powder was supplied at the inlet of pipe under the condition of 6 m/s argon gas flow rate. A reference zone was defined underneath the pipe outlet. The particle concentration in the reference zone was quantified and then compared with experiment results. In order to clearly observe the pre-mixed powder distribution in argon gas flow, ten different sections in powder feeder pipe were selected, which were depicted in Figure 5. The powder distributions in the ten pipe sections shown in Figure 6 were at the moment of 5 second. From section1 to section10, it can be observed that both two powders moved forward uniformly and kept the original mixing composition ratio approximately. There was not clear separation phenomenon of pre-mixed powder in all the ten sections. The simulation result indicated that both 4047 Al particles and Cu particles had almost uniform velocities. Through optimizing particle diameter, the Al particles had bigger particle size but less density, while Cu particles had smaller particle size but greater

density, so the product of particle density and particle diameter square in Eqn.1 was close to be same for all the particles in pre-mixed powder. Therefore, all the particles had almost same accelerations under the identical argon gas flow. The initial velocity for any particle was supposed to be zero at the inlet of feeder pipe. As a result, all the particles gained almost uniform velocity. The simulation result showed that pre-mixed powder separation was effectively controlled and all the powders moved along powder feeder pipe neck and neck.

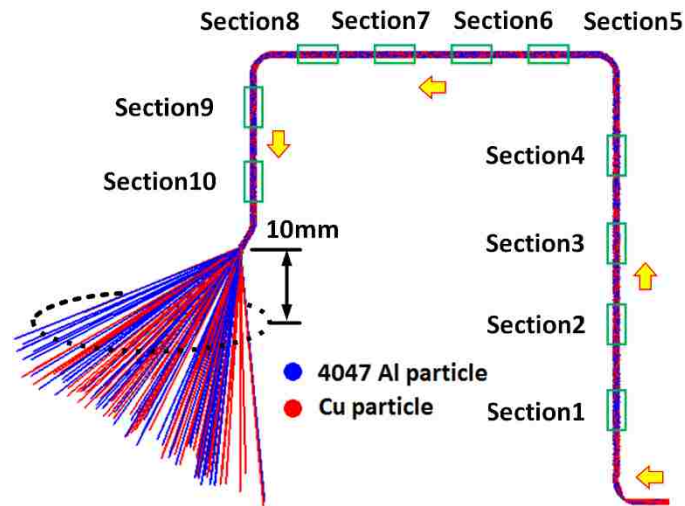


Figure 5. The powder distribution in simulation result and ten sections

In order to observe how the particle distribution changed over time, the particle distribution in the section1 and section3 at five different moments were depicted in Figure 7. The time interval between two adjacent moments was 0.05 second. The section1 located close to powder feeder inlet. By observing the particle distributions in section1, it can be found that both 4047 Al particles and Cu particles had tendency to move forward with almost uniform mixing composition ratio. This tendency totally continued in the section3. At the successive five moments, powder mixture gradually started to disperse but still kept

uniform mixing ratio. Powder separation was not found in the particle distribution changed over time. The particle size optimization method can eliminate the powder separation effectively.

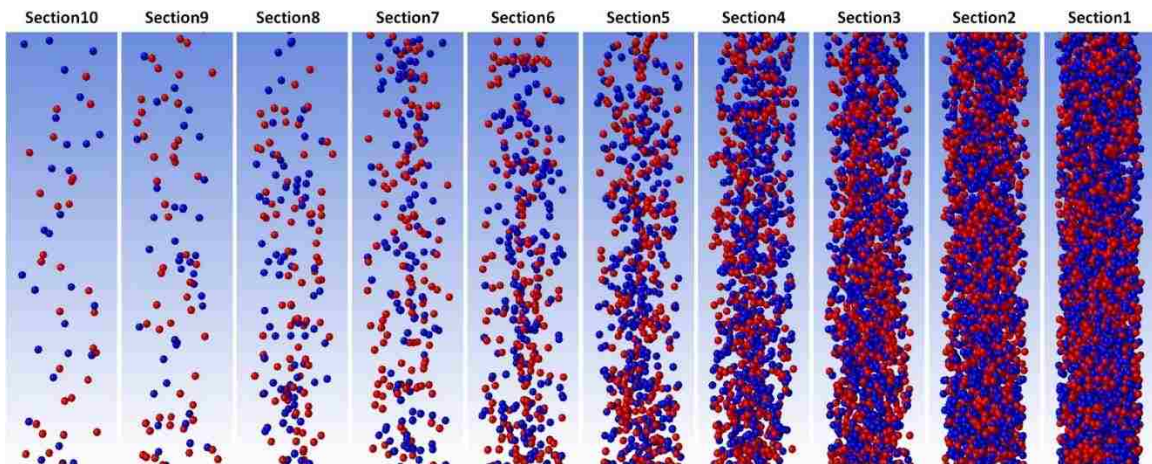


Figure 6. The simulated powder distribution results in ten sections.

The particle volume percentages in the reference zone were quantified and plotted in Figure 8. Green color recorded the volume percentage of 4047 Al, while purple color recorded the volume percentage of Cu. The time in the X-axis indicated the moments when the exiting particles from nozzle reached the reference zone. The time started when the first particle was blown to move at the inlet. In the beginning stage (approximately 0s ~ 4s), no particle sprayed out from the nozzle, so the volume percentage of two powders was zero. Starting from the moment of 4s, a flow of 4047 Al powder and Cu powder mixture exited from the nozzle. The volume percent of Cu was slightly greater than Al powder. But after about 2 seconds, Al powder volume percent surpassed Cu volume percent and kept greater than Cu volume percent for about 6 seconds. Then both powder volume percentages oscillated and alternate with time went by. An interesting result was both powder volume

percentages oscillated near the 50% standard line. That means pre-mixed powder did not separate and kept almost uniform as being blown in powder feeder pipe. Through optimizing particle size, pre-mixed powder separation can be effectively controlled based on the modeling results.

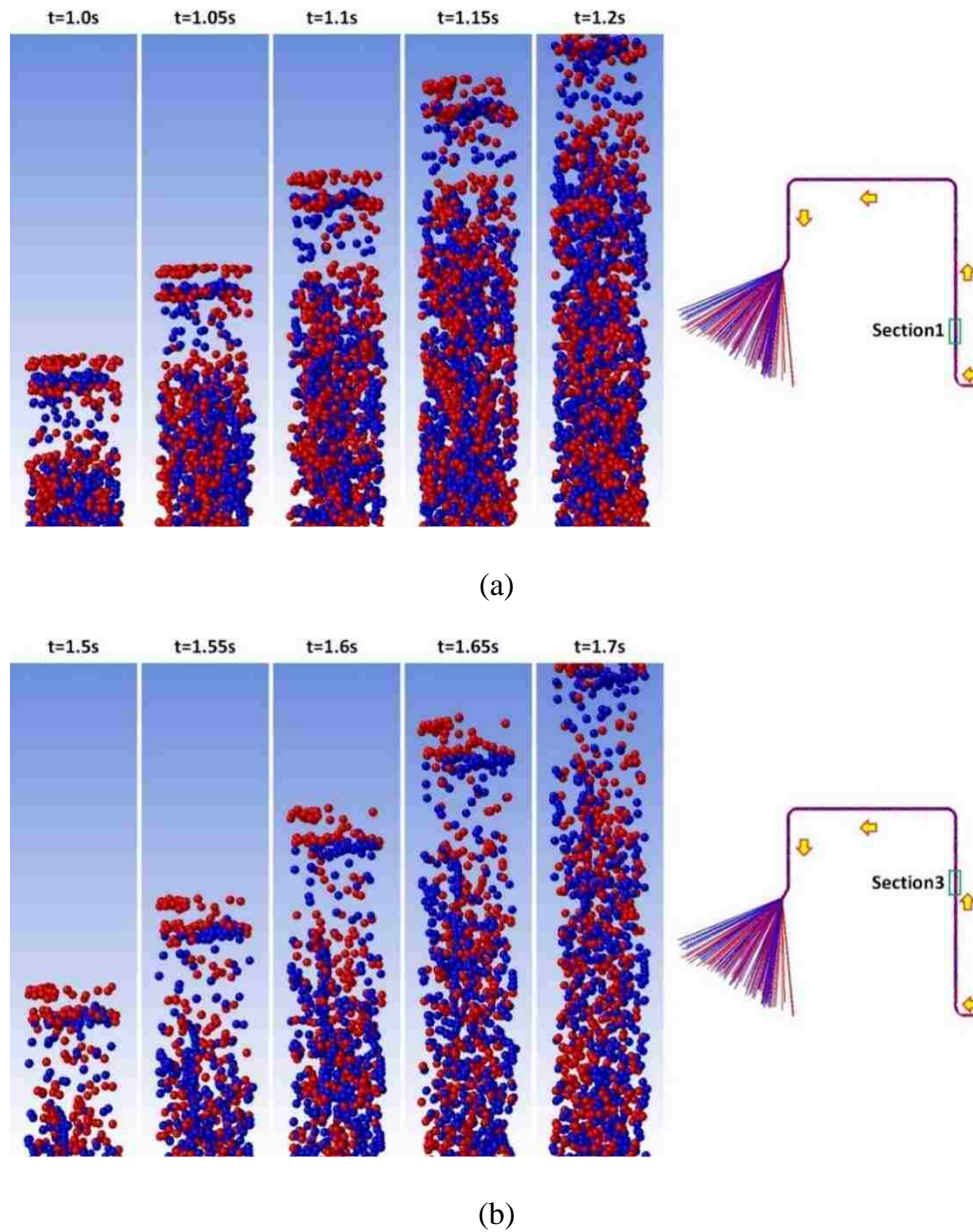


Figure 7. The powder distribution in (a). section1 and (b). section3 at different moments.

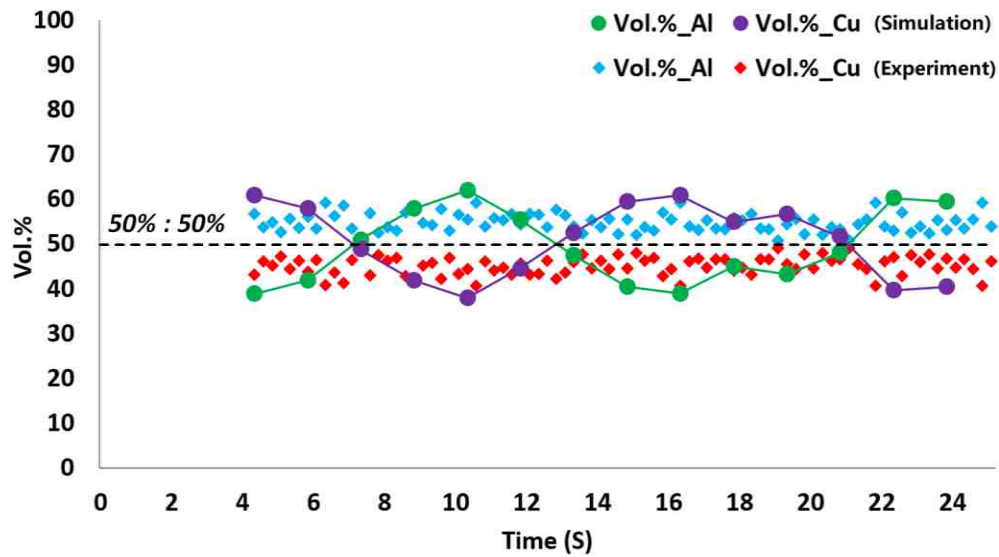


Figure 8. Simulation results and experimental validation.

The experimental validation of simulated results with optimized particle size was depicted in Figure 8. The vacant period in the simulation was same with the experiment result. Starting from the moment of 4s, a flow of 4047 Al powder and Cu powder mixture exited from the nozzle. In the simulation result, both powder volume percentages oscillated and alternated with time went by. And both powder volume percentages oscillated near the 50% standard line. That means pre-mixed powder did not separate and kept almost uniform as being blown in powder feeder pipe. In the experimental result, the powder's volume percentages also showed oscillations near 50% standard line. However, there were not alternations of 4047 Al and Cu powder volume percentages compared with the simulation results. Al powder volume percentage was always greater than Cu powder. By analyzing the optimized pre-mixed powder's composition distribution simulated with model and patterned in the epoxy resin coating, the powder flow had basically stable volume percentages, which were close to 50%:50%. Through optimizing particle size, pre-mixed

powder separation can be effectively controlled, which was clearly found in both simulation and experimental results.

4. CONCLUSION

This study presented a comprehensive CFD-DEM model to investigate the particle size optimization's effect on controlling pre-mixed powder flow separation. In the simulated results with optimized particle size, both powder volume percentages alternated with time went by and oscillated near the 50% standard line. The pre-mixed powder did not separate and kept almost uniform as being blown in powder feeder pipe. The modeled powder volume percentages showed alternation and oscillation near the 50% line, which can be validated by experimental powder volume percentages. Through optimizing particle size, pre-mixed powder separation can be effectively controlled, which was clearly found in both simulation and experimental results.

REFERENCES

- [1] Li, W., Zhang, J., Zhang, X., and Liou, F., 2017, "Effect of optimizing particle size on directed energy deposition of Functionally Graded Material with blown Pre-Mixed Multi-Powder," *Manufacturing Letters*, 13, pp. 39-43.
- [2] Carroll, B. E., Otis, R. A., Borgonia, J. P., Suh, J.-o., Dillon, R. P., Shapiro, A. A., Hofmann, D. C., Liu, Z.-K., and Beese, A. M., 2016, "Functionally graded material of 304L stainless steel and inconel 625 fabricated by directed energy deposition: Characterization and thermodynamic modeling," *Acta Materialia*, 108, pp. 46-54.
- [3] Schwendner, K. I., Banerjee, R., Collins, P. C., Brice, C. A., and Fraser, H. L., 2001, "Direct laser deposition of alloys from elemental powder blends," *Scripta Materialia*, 45(10), pp. 1123-1129.

- [4] Li, W., Yan, L., Karnati, S., Liou, F., Newkirk, J., Taminger, K. M. B., and Seufzer, W. J., 2017, "Ti-Fe intermetallics analysis and control in joining titanium alloy and stainless steel by Laser Metal Deposition," *Journal of Materials Processing Technology*, 242, pp. 39-48.
- [5] Li, W., Chen, X., Yan, L., Zhang, J., Zhang, X., and Liou, F., 2017, "Additive manufacturing of a new Fe-Cr-Ni alloy with gradually changing compositions with elemental powder mixes and thermodynamic calculation," *The International Journal of Advanced Manufacturing Technology*.
- [6] Li, W., Yan, L., Chen, X., Zhang, J., Zhang, X., and Liou, F., 2018, "Directed energy depositing a new Fe-Cr-Ni alloy with gradually changing composition with elemental powder mixes and particle size effect in fabrication process," *Journal of Materials Processing Technology*, 255, pp. 96-104.
- [7] Wen, S., Shin, Y., Murthy, J., and Sojka, P., 2009, "Modeling of coaxial powder flow for the laser direct deposition process," *International Journal of Heat and Mass Transfer*, 52(25), pp. 5867-5877.
- [8] Li, W., Liou, F., Newkirk, J., Taminger, K. M. B., and Seufzer, W. J., 2017, "Investigation on Ti6Al4V-V-Cr-Fe-SS316 Multi-layers Metallic Structure Fabricated by Laser 3D Printing," *Scientific Reports*, 7.
- [9] Zhu, H., Zhou, Z., Yang, R., and Yu, A., 2008, "Discrete particle simulation of particulate systems: a review of major applications and findings," *Chemical Engineering Science*, 63(23), pp. 5728-5770.
- [10] Zhao, J., and Shan, T., 2013, "Coupled CFD-DEM simulation of fluid-particle interaction in geomechanics," *Powder technology*, 239, pp. 248-258.
- [11] Parteli, E. J., and Pöschel, T., 2016, "Particle-based simulation of powder application in additive manufacturing," *Powder Technology*, 288, pp. 96-102.
- [12] Haeri, S., Wang, Y., Ghita, O., and Sun, J., 2017, "Discrete element simulation and experimental study of powder spreading process in additive manufacturing," *Powder Technology*, 306, pp. 45-54.
- [13] Guide, A. F. U., 2011, "Release 14.0, ANSYS Fluent User Manual," Inc., November.
- [14] Parteli, E. J., 2013, "Using LIGGGHTS for performing DEM simulations of particles of complex shapes with the multisphere method," In: *DEM6-6th International Conference on Discrete Element Methods and Related Techniques*, Golden USA.

- [15] Kloss, C., Goniva, C., Hager, A., Amberger, S., and Pirker, S., 2012, "Models, algorithms and validation for opensource DEM and CFD-DEM," *Progress in Computational Fluid Dynamics, an International Journal*, 12(2-3), pp. 140-152.
- [16] Zekovic, S., Dwivedi, R., and Kovacevic, R., 2007, "Numerical simulation and experimental investigation of gas-powder flow from radially symmetrical nozzles in laser-based direct metal deposition," *International Journal of Machine Tools and Manufacture*, 47(1), pp. 112-123.
- [17] Thompson, S. M., Bian, L., Shamsaei, N., and Yadollahi, A., 2015, "An overview of Direct Laser Deposition for additive manufacturing; Part I: Transport phenomena, modeling and diagnostics," *Additive Manufacturing*, 8, pp. 36-62.
- [18] Li, W., Karnati, S., Zhang, Y., and Liou, F., 2018, "Investigating and eliminating powder separation in pre-mixed powder supply for laser metal deposition process," *Journal of Materials Processing Technology*, 254, pp. 294-301.
- [19] Morsi, S., and Alexander, A., 1972, "An investigation of particle trajectories in two-phase flow systems," *Journal of Fluid mechanics*, 55(02), pp. 193-208.
- [20] Pan, H., Sparks, T., Thakar, Y. D., and Liou, F., 2006, "The investigation of gravity-driven metal powder flow in coaxial nozzle for laser-aided direct metal deposition process," *Journal of manufacturing science and engineering*, 128(2), pp. 541-553.
- [21] Lia, W., Zhanga, J., Karnatia, S., Zhanga, Y., Lioua, F., Newkirkb, J., Tamingerc, K., and Seufzerc, W., "MODELING AND EXPERIMENTAL INVESTIGATION OF PRE-MIXED MULTI-POWDER FLOW IN FABRICATING FUNCTIONAL GRADIENT MATERIAL BY LASER METAL DEPOSITION PROCESS."
- [22] Serag-Eldin, M., and Spalding, D., 1979, "Computations of three-dimensional gas-turbine combustion chamber flows," *Journal of Engineering for Power*, 101(3), pp. 326-336.
- [23] Launder, B. E., and Spalding, D. B., 1972, "Lectures in mathematical models of turbulence."

SECTION

2. CONCLUSION

This dissertation investigated the pre-mixed powder flow behaviors in powder feeder pipe with both experimental and modeling approaches. The main conclusions can be summarized as follows.

In the pre-mixed powders, which have two types of powder with different densities, if the particle diameter ratio is equal to or close to an ideal value, all the particles will have the same acceleration when moving in powder feeder pipe. The ideal value is the square root of powder density ratio. Therefore, there will be very less powder separation. The designed composition in pre-mixed powder can be maintained.

Otherwise, if the particle diameter ratio is much greater or less than the ideal value, powder separation will happen in powder feeder pipe due to the different particle accelerations. It will cause the deviation between original composition and real composition. The designed composition in pre-mixed powder will be ruined.

Powder delivered by argon gas flow is a typical fluid-particle system. In this system, particle or granular material's motion is caused or driven by the fluid medium's flow motion and fluctuation. An encouraging modeling approach to investigate the above fluid-particle system is a coupled Computational Fluid Dynamics method and Discrete Element Method (CFD-DEM), which properly considers the interaction of fluid and particle. By solving discrete particle acceleration equations coupled with continuity equations and momentum equations for argon gas, the dynamic behavior of pre-mixed flow was simulated.

In pre-mixed powder with Cu and 4047 Al powder, since Al particle has smaller particle size and lighter density than Cu particle, the acceleration of Al particle was greater than Cu particle, so that Al particle moved faster than Cu particle. The separation phenomenon in pre-mixed powder was observed in both modeling result and experiment. The pre-mixed powder separation generated the intersection point of Al and Cu powder volume percentage plots. A noteworthy result is the intersection point with higher argon gas flow rate appeared earlier than the intersection point with lower argon gas flow rate. It was because higher argon gas flow rate caused bigger drag force to particles. As a result, powder separation occurred much faster than lower argon gas flow rate.

BIBLIOGRAPHY

- [1] Li, W., Zhang, J., Zhang, X., and Liou, F., 2017, "Effect of optimizing particle size on directed energy deposition of Functionally Graded Material with blown Pre-Mixed Multi-Powder," *Manufacturing Letters*, 13, pp. 39-43.
- [2] Li, W., Karnati, S., Zhang, Y., and Liou, F., 2018, "Investigating and eliminating powder separation in pre-mixed powder supply for laser metal deposition process," *Journal of Materials Processing Technology*, 254, pp. 294-301.
- [3] Li, W., Chen, X., Yan, L., Zhang, J., Zhang, X., and Liou, F., 2017, "Additive manufacturing of a new Fe-Cr-Ni alloy with gradually changing compositions with elemental powder mixes and thermodynamic calculation," *The International Journal of Advanced Manufacturing Technology*.
- [4] Li, W., Yan, L., Karnati, S., Liou, F., Newkirk, J., Taminger, K. M. B., and Seufzer, W. J., 2017, "Ti-Fe intermetallics analysis and control in joining titanium alloy and stainless steel by Laser Metal Deposition," *Journal of Materials Processing Technology*, 242, pp. 39-48.
- [5] Carroll, B. E., Otis, R. A., Borgonia, J. P., Suh, J.-o., Dillon, R. P., Shapiro, A. A., Hofmann, D. C., Liu, Z.-K., and Beese, A. M., 2016, "Functionally graded material of 304L stainless steel and inconel 625 fabricated by directed energy deposition: Characterization and thermodynamic modeling," *Acta Materialia*, 108, pp. 46-54.
- [6] Li, W., Liou, F., Newkirk, J., Taminger, K. M. B., and Seufzer, W. J., 2017, "Investigation on Ti6Al4V-V-Cr-Fe-SS316 Multi-layers Metallic Structure Fabricated by Laser 3D Printing," *Scientific Reports*, 7.
- [7] Li, W., Karnati, S., Kriewall, C., Liou, F., Newkirk, J., Taminger, K. M. B., and Seufzer, W. J., 2017, "Fabrication and Characterization of a Functionally Graded Material from Ti-6Al-4 V to SS316 by Laser Metal Deposition," *Additive Manufacturing*.
- [8] Zhu, H., Zhou, Z., Yang, R., and Yu, A., 2008, "Discrete particle simulation of particulate systems: a review of major applications and findings," *Chemical Engineering Science*, 63(23), pp. 5728-5770.
- [9] Li, W., Yan, L., Chen, X., Zhang, J., Zhang, X., and Liou, F., 2018, "Directed energy depositing a new Fe-Cr-Ni alloy with gradually changing composition with elemental powder mixes and particle size effect in fabrication process," *Journal of Materials Processing Technology*, 255, pp. 96-104.

- [10] Zhao, J., and Shan, T., 2013, "Coupled CFD–DEM simulation of fluid–particle interaction in geomechanics," *Powder technology*, 239, pp. 248-258.
- [11] Parteli, E. J., and Pöschel, T., 2016, "Particle-based simulation of powder application in additive manufacturing," *Powder Technology*, 288, pp. 96-102.
- [12] Haeri, S., Wang, Y., Ghita, O., and Sun, J., 2017, "Discrete element simulation and experimental study of powder spreading process in additive manufacturing," *Powder Technology*, 306, pp. 45-54.
- [13] Guide, A. F. U., 2011, "Release 14.0, ANSYS Fluent User Manual," Inc., November.
- [14] Parteli, E. J., 2013, "Using LIGGGHTS for performing DEM simulations of particles of complex shapes with the multisphere method," In: *DEM6-6th International Conference on Discrete Element Methods and Related Techniques*, Golden USA.
- [15] Kloss, C., Goniva, C., Hager, A., Amberger, S., and Pirker, S., 2012, "Models, algorithms and validation for opensource DEM and CFD–DEM," *Progress in Computational Fluid Dynamics, an International Journal*, 12(2-3), pp. 140-152.
- [16] Zekovic, S., Dwivedi, R., and Kovacevic, R., 2007, "Numerical simulation and experimental investigation of gas–powder flow from radially symmetrical nozzles in laser-based direct metal deposition," *International Journal of Machine Tools and Manufacture*, 47(1), pp. 112-123.
- [17] Thompson, S. M., Bian, L., Shamsaei, N., and Yadollahi, A., 2015, "An overview of Direct Laser Deposition for additive manufacturing; Part I: Transport phenomena, modeling and diagnostics," *Additive Manufacturing*, 8, pp. 36-62.
- [18] Wen, S., Shin, Y., Murthy, J., and Sojka, P., 2009, "Modeling of coaxial powder flow for the laser direct deposition process," *International Journal of Heat and Mass Transfer*, 52(25), pp. 5867-5877.
- [19] Lia, W., Zhanga, J., Karnatia, S., Zhanga, Y., Lioua, F., Newkirkb, J., Tamingerc, K., and Seufzerc, W., "MODELING AND EXPERIMENTAL INVESTIGATION OF PRE-MIXED MULTI-POWDER FLOW IN FABRICATING FUNCTIONAL GRADIENT MATERIAL BY LASER METAL DEPOSITION PROCESS."
- [20] Morsi, S., and Alexander, A., 1972, "An investigation of particle trajectories in two-phase flow systems," *Journal of Fluid mechanics*, 55(02), pp. 193-208.
- [21] Pan, H., Sparks, T., Thakar, Y. D., and Liou, F., 2006, "The investigation of gravity-driven metal powder flow in coaxial nozzle for laser-aided direct metal deposition process," *Journal of manufacturing science and engineering*, 128(2), pp. 541-553.

VITA

Wei Li was born in Salaqi, Inner Mongolia, China. He received his Bachelor of Science degree in Mechanical Engineering in June 2005 from University of Electronics Science and Technology of China, Chengdu, China. In April 2012, he received his first Master of Science degree in Engineering Mechanics from Tongji University, Shanghai, China. In July 2017, he received his second Master of Science degree in Manufacturing Engineering from Missouri University of Science and Technology, Rolla, Missouri, USA. In August 2018, he received his Doctor of Philosophy in Mechanical Engineering from Missouri University of Science and Technology, Rolla, Missouri, USA.

During his Ph.D study, he won the third place award in the Intelligent System Center (ISC) Graduate Research Symposium for twice (2016, 2017 respectively). In 2018, he was awarded as College of Engineering and Computing (CEC) Dean's Ph.D Scholar, not only for his scholarly contributions, but also for his academic success and service contributions. During his Ph.D. study, he was awarded a US patent application, a NASA technology transfer, authored and co-authored 18 journal papers, 9 conference papers, and one book chapter.